

© 2017 Tonghui Cui

OPTIMAL DESIGN OF UNMODELED LINEAR SYSTEMS USING
CONTROL-BASED CONTINUATION

BY

TONGHUI CUI

THESIS

Submitted in partial fulfillment of the requirements
for the degree of Master of Science in Mechanical Engineering
in the Graduate College of the
University of Illinois at Urbana-Champaign, 2017

Urbana, Illinois

Adviser:

Professor Harry Dankowicz

ABSTRACT

This thesis describes the use of control-based continuation for design optimization, in the presence of constraints and without access to a model, of the response of a linear system to harmonic input. A proof of concept of this paradigm is presented in the context of an armature-controlled DC motor. Specifically, three design problems are formulated with the objective function equal to the maximum angular velocity response to a harmonic torque disturbance, and a constraint that is imposed on each of three distinct stability margins, respectively. The analysis shows that the simulation model for the DC motor may be treated analogously to an actual experiment with all information drawn from real-time measurements, rather than from the model itself. The control-based continuation paradigm is formulated in terms of a non-invasive, yet locally stabilizing control scheme, which can be tuned to accelerate convergence to the steady state response. The numerical analysis uses the MATLAB-compatible continuation platform COCO to determine the implicit relationship between model parameters that results from the constraint, and to evaluate the objective function along the corresponding constraint manifold. A comparison between a scheme that relies on finite differences for approximating the problem Jacobian and an algorithm based on the Broyden update is also included.

To my parents, for their love and support.

ACKNOWLEDGMENTS

I would first like to thank my thesis advisor Prof. Harry Dankowicz. He taught me not only the skills but also the qualities one need to be a researcher. During the time of this research, he consistently allowed this thesis to be my own work, but is always there when I need help.

I would also like to thank Kathy Smith in the Graduate Programs Office of the Department of Mechanical Science and Engineering. She is always nice to students and always reminded me of the deadlines I could not afford to miss.

Finally, I must express my gratitude to my parents and to my wife for providing me with unfailing support and continuous encouragement throughout my years of study and through the process of researching and writing this thesis. This accomplishment would not have been possible without them. Thank you.

TABLE OF CONTENTS

CHAPTER 1	INTRODUCTION	1
1.1	Design and Optimization	1
1.2	Linear Systems	2
1.3	Parameter Continuation	2
1.4	Control-Based Continuation	4
1.5	Contribution and Outline	5
CHAPTER 2	PROBLEM FORMULATION	7
2.1	Mathematical Model	7
2.2	Design Criteria	12
2.3	Discussion	16
CHAPTER 3	ALGEBRAIC CONTINUATION	17
3.1	Constant Gain Margin	17
3.2	Constant Phase Margin	21
3.3	Constant Nyquist Distance	25
3.4	Discussion	29
CHAPTER 4	CONTROL-BASED CONTINUATION	31
4.1	Elementary Experiments	31
4.2	Frequency Sweeps	36
4.3	Constant Gain Margin	49
4.4	Constant Phase Margin	53
4.5	Constant Nyquist Distance	55
4.6	Discussion	59
CHAPTER 5	THE CONTINEX TOOLBOX	61
5.1	Numerical Results	61
CHAPTER 6	CONCLUSIONS	67
APPENDIX A	CONTINEX-COMPATIBLE IMPLEMENTATION OF ELEMENTARY EXPERIMENTS	69

APPENDIX B IMPLEMENTATION OF COUPLED CONTIN-	
UATION PROBLEMS USING CONTINEX	73
B.1 Constant Gain Margin	73
B.2 Constant Phase Margin	74
B.3 Constant Nyquist Distance	75
REFERENCES	78

CHAPTER 1

INTRODUCTION

This study focuses on the combination of a numerical method with feedback control for design optimization of an unmodeled system. In particular, the analysis seeks to identify parameters of an armature-controlled DC motor [24] to improve disturbance rejection performance under constraints on the stability of the system.

This chapter serves as an essential introduction to the topics discussed in this study. This includes the necessary background for implementing parameter continuation in problems where an explicit model may or may not be available. Also included is a brief literature review about control-based continuation. A summary of the contributions of this thesis and an outline conclude the chapter.

1.1 Design and Optimization

In engineering design, parameters that govern a system are adjusted until the system performance meets desired requirements while satisfying predefined constraints [13]. Optimization is a process of selecting from all the possible designs an optimal choice that maximizes or minimizes a suitably defined objective function. Different collections of constraints may lead to different optimal designs, even for the same objective function.

In the absence of constraints, when the relationship between the adjustable parameters and the objective function is explicitly available, it may be possible to find the optimal design choice analytically. When constraints are present, the adjustable parameters are no longer independent, and it may be very difficult to eliminate the constraints by restricting to a smaller number of independent parameters [19]. Instead, numerical methods must be used to explore the design space.

A further complication arises when neither the constraints nor the objective function can be expressed explicitly in terms of the adjustable parameters. In this case, experiments must be integrated in the process of optimization [22].

1.2 Linear Systems

The steady-state response of a harmonically excited, stable, linear, time-invariant system is harmonic with the same frequency [25]. The function that describes the response amplitude and phase is the frequency response function [15]. The frequency response function can be used to characterize the sensitivity of a system to disturbances. Similarly, the stability of a dynamical system with closed-loop feedback may be evaluated in terms of properties of the frequency response function of a suitably defined open-loop dynamical system.

For example, the gain margin of the closed-loop system is defined as the ratio of the maximum possible gain that preserves stability to the actual system gain [33]. It can be measured at the phase crossover frequency when the phase of the open-loop frequency response function equals $-\pi$. Similarly, the phase margin is measured at the gain crossover frequency when the amplitude of the open-loop frequency response function equals 1.

In this thesis, we consider design and optimizations problems formulated in terms of the frequency response functions of several linear systems. For example, we analyze an objective function defined in terms of the maximum response amplitude for one frequency response function under constraints imposed on the gain or phase margin of another frequency response function.

1.3 Parameter Continuation

This thesis considers only equality constraints corresponding to equations in terms of the system properties. Continuous families of solutions to such equations may be analyzed using the method of parameter continuation. We use the canonical formulation of the extended continuation problem described in [10]. Specifically, let the function $\Phi : \mathbb{R}^n \rightarrow \mathbb{R}^m$, where $n \geq m \geq 1$, be

continuously differentiable. The equation $\Phi(u) = 0$ is a *zero problem* in the vector u of continuation variables and represents the constraints on the design problem. Consider, in addition, a set of *monitor functions* denoted by $\Psi : \mathbb{R}^n \rightarrow \mathbb{R}^r$ that include the objective function. The *extended continuation problem* is then defined as $F(u, \kappa) = 0$, where

$$F : (u, \kappa) \mapsto \begin{pmatrix} \Phi(u) \\ \Psi(u) - \kappa \end{pmatrix}. \quad (1.1)$$

Further, let $\mathbb{I} \in \{1, \dots, r\}$ be an *index set* of cardinality $|\mathbb{I}| \leq n - m$. Its complement is denoted by $\mathbb{J} := \{1, \dots, r\} \setminus \mathbb{I}$. Given a constant $\kappa_{\mathbb{I}}^*$, the restriction $G : \mathbb{R}^{n+r-|\mathbb{I}|} \rightarrow \mathbb{R}^{m+r}$, where

$$G : (u, \kappa_{\mathbb{J}}) \mapsto F(u, \kappa) \big|_{\kappa_{\mathbb{I}} = \kappa_{\mathbb{I}}^*}, \quad (1.2)$$

defines the restricted continuation problem $G(u, \kappa_{\mathbb{J}}) = 0$. Every regular solution point of the restricted continuation problem lies on a locally unique $n - m - |\mathbb{I}|$ -dimensional solution manifold.

A restricted continuation problem is initialized with an initial solution guess u_0 , such that $\kappa_{\mathbb{J}} = \Psi_{\mathbb{J}}(u_0)$. The entries of the vector $\kappa_{\mathbb{I}}^*$ may either be initialized with the entries of $\Psi_{\mathbb{I}}(u_0)$, or assigned some other preferred values.

Given an initial solution guess, the restricted continuation problem may be solved numerically by application of Newton's method. In general, the solution to the equation $f(x) = 0$ may be approximated by the limit of a sequence

$$x_{n+1} = x_n - j_n^{-1} f(x_n), \quad (1.3)$$

where j_n is an approximation to the Jacobian $Df(x_n)$. In the Broyden update method,

$$j_n = j_{n-1} + \frac{(f(x_n) - f(x_{n-1})) - j_{n-1}^{-1}(x_n - x_{n-1})}{\|(x_n - x_{n-1})\|} (x_n - x_{n-1})^T. \quad (1.4)$$

In this case, j_0 may be initialized arbitrarily, for example, using a matrix obtained from a related problem.

A continuation algorithm combines a nonlinear solver, such as the Newton method, with a method for generating new solutions on the solution manifold from existing solutions.

1.4 Control-Based Continuation

As suggested previously, it may be necessary to perform an experiment in order to evaluate the zero and monitor functions of a restricted continuation problem. This requires that the outcome of the experiment can be uniquely associated to the values of the continuation variables. For example, in a linear system, the frequency response function is uniquely parameterized by the system parameters and the excitation frequency, independently of the initial conditions, and measurable using an experiment, provided that convergence to the steady state is achieved.

The rate of convergence to the steady-state response may be regulated by the addition of feedback control with adjustable gains. Such a feedback scheme is said to be noninvasive if the control input equals 0 when the system is in steady state [4]. When combined with parameter continuation, such an implementation is called control-based continuation. The literature on this topic is relatively young (e.g., [26]) and its application to constrained design optimization has yet to be explored (but see [2]).

A general setup of control-based continuation includes sensors that collect measurements from the experiment and a computer with an embedded numerical algorithm that applies the nonlinear solver and manifold continuation method to locate successive points on the solution manifold. Experiments are repeated with the updated setup until the continuation is completed.

In 2008, Sieber and Krauskopf [29] explores control-based continuation in simulations by investigating an autonomous dry friction oscillator. They successfully tracked periodic responses of the nonlinear oscillator, as well as associated bifurcations, using just the output of a simulation. In another work [30], they illustrated the use of control-based continuation for studying the periodic response of a pendulum with axis of rotation suspended on a mass-spring-damper system. Specifically, they suggested that control-based continuation could be applied to a hybrid substructured model, with a simulated mass-spring-damper system interacting with a physical model of the pendulum through an appropriate actuator. The formulation showed that delay-induced instability of the hybrid test could be eliminated by a suitable identification of the continuation variables and zero functions. The first application of control-based continuation in an actual experiment was achieved by Sieber *et al.* [31]. In this paper, a saddle-node bifurcation of periodic

orbits was tracked successfully for a vertically forced pendulum.

Inspired by Sieber and Krauskopf, Barton and Burrow [2] used control-based continuation in a physical experiment to track a branch of periodic orbits of a nonlinear energy harvester through a saddle-node bifurcation. The bistable spring characteristics of this harvester were explored further in [3], where a bifurcation diagram obtained using control-based continuation was validated against the result of harmonic balance applied to an explicit mathematical model of the system dynamics.

The control-based continuation method was applied in an equation-free bifurcation analysis of an idealized traffic jam model by Marschler *et al.* [16, 17]. Another interesting application was discussed by Krauskopf and Sieber [21], where they performed a bifurcation analysis of the EI-Nino Southern Oscillation. An even more complicated application of control-based continuation was backbone curve identification, proposed by Renson *et al.* [23] as an alternative to the resonant-decay approach, in which amplitude-dependent characteristics of the system are extracted experimentally from the free response.

A detailed investigation of the algorithmic nature of a control-based continuation scheme, the sensitivity to experimental noise, and methods for approximating the problem Jacobian has been performed in a series of papers by Bureau *et al.* [6, 7, 8, 9, 27] on a piecewise smooth oscillator. The authors present a systematic method for tuning the feedback gains and discuss three methods for on-the-fly evaluation of the uncontrolled stability of periodic responses of the oscillator. Moreover, they describe the implementation of their control-based continuation algorithm in the CONTINEX toolbox, compatible with the MATLAB-based continuation platform COCO [28].

1.5 Contribution and Outline

This thesis makes an original contribution to the literature by applying the method of control-based continuation to an example linear dynamical system in order to show how this approach can be integrated with design optimization in the presence of constraints and without access to an explicit model.

The system of interest in this thesis is a DC motor. Three design problems are proposed in terms of two model parameters, constraints on suitably defined stability margins, and an objective function characterizing the mini-

imum disturbance rejection. Numerical results of control-based continuation are validated against the predictions from parameter continuation performed on explicit expressions for the zero functions and monitor functions.

The proposed method and simulation strategies in this thesis generalize to arbitrary linear, time-invariant systems, and may also give insight into design analysis for time-varying systems and nonlinear systems.

The remainder of this thesis is organized as follows. Chapter 2 introduces the model of the DC motor and derives analytical expressions for the frequency response functions of interest. These are used to propose the three design problems associated with constant gain margin, constant phase margin, and constant Nyquist distance, respectively. In Chapter 3, the algebraic systems of equations obtained in Chap. 2 for each of the three design problems are analyzed numerically using COCO.

In Chap. 4, the DC motor is considered as a black box represented by a SIMULINK model with adjustable inputs and measurable outputs. The control-based continuation approach is used to reformulate the design problems in terms of computable zero and monitor functions. These are then analyzed with COCO and the results are compared to the predictions from Chap. 3. A slight variation is introduced in Chap. 5, where the implementation of Broyden's method in CONTINEX is used during continuation.

The thesis concludes with a brief summary and a discussion about possible future research.

CHAPTER 2

PROBLEM FORMULATION

In this chapter, we develop the general design methodology introduced in Chap. 1 in the context of the dynamics of a linear, armature-controlled DC motor with an integrator in the feedback loop and driven by a reference angular velocity. We formulate three distinct design problems amenable to parameter continuation. In each case, a constraint is imposed on the Nyquist curve for the open-loop transfer function, and optimization seeks to minimize the amplitude of the steady-state response to a harmonic torque disturbance.

2.1 Mathematical Model

To illustrate the methodology, consider the following model of an armature controlled DC motor [24]:

$$J\omega'(t) + b\omega(t) = K_t i(t) + \lambda(t), \quad (2.1)$$

$$Li'(t) + Ri(t) = v(t) - K_e\omega(t), \quad (2.2)$$

where $\omega(t)$ is the angular velocity of the motor shaft at time t , $i(t)$ is the current through the armature, $v(t)$ is the driving voltage applied to the motor, and $\lambda(t)$ is a disturbance torque on the motor shaft. The parameters J , b , L , and R represent the shaft moment of inertia about its axis of rotation, the viscous damping coefficient, the armature inductance, and the armature resistance, respectively. The proportionality constants K_t and K_e relate current to the induced torque and angular velocity to the back emf, respectively. This system of coupled differential equations models the response of the armature current and the shaft's angular velocity to variations in the applied voltage and the presence of the disturbance torque. For example, for constant voltage $V(t) \equiv V_0$ and zero disturbance, $\lambda(t) \equiv 0$, the steady

state angular velocity equals $K_t V_0 / (bR + K_e K_t)$, corresponding to a constant current $i(t) \equiv bV_0 / (bR + K_e K_t)$.

Since the model is linear with constant coefficients, it is convenient to transform the description to the frequency domain, such that

$$Js\Omega(s) + b\Omega(s) - K_t I(s) = \Lambda(s) + J\omega_0, \quad (2.3)$$

$$K_e \Omega(s) + LsI(s) + RI(s) = V(s) + Li_0, \quad (2.4)$$

where $\Omega(s)$, $I(s)$, $V(s)$, and $\Lambda(s)$ are the corresponding Laplace transforms, $\omega_0 = \omega(0)$, and $i_0 = i(0)$. This implies that

$$\Omega(s) = \frac{K_t Li_0 + (R + Ls)(J\omega_0 + \Lambda(s)) + K_t V(s)}{(b + Js)(R + Ls) + K_e K_t}, \quad (2.5)$$

$$I(s) = \frac{-K_e J\omega_0 + (b + Js)(Li_0 + V(s)) - K_e \Lambda(s)}{(b + Js)(R + Ls) + K_e K_t}. \quad (2.6)$$

It follows that the voltage-to-angular velocity transfer function equals

$$H_{V \rightarrow \Omega}(s) := \frac{K_t}{(b + Js)(R + Ls) + K_e K_t}, \quad (2.7)$$

whereas the voltage-to-current transfer function equals

$$H_{V \rightarrow I}(s) := \frac{b + Js}{(b + Js)(R + Ls) + K_e K_t}. \quad (2.8)$$

Similarly, the disturbance torque-to-angular velocity transfer function equals

$$H_{\Lambda \rightarrow \Omega} := \frac{R + Ls}{(b + Js)(R + Ls) + K_e K_t} \quad (2.9)$$

and the disturbance torque-to-current transfer function equals

$$H_{\Lambda \rightarrow I}(s) := -\frac{K_e}{(b + Js)(R + Ls) + K_e K_t}. \quad (2.10)$$

A corresponding system representation is shown in the block diagram below (Fig. 2.1).

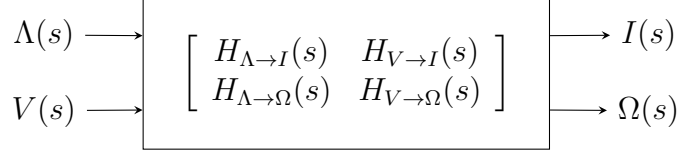


Figure 2.1: System representation of the DC motor.

2.1.1 Time-domain responses

Let $h(t)$ denote the inverse Laplace transform of $[(b + Js)(R + Ls) + K_e K_t]^{-1}$. If $(bL + RJ)^2 \neq 4JL(bR + K_e K_t)$, then

$$h(t) = \frac{e^{\sigma_1 t} - e^{\sigma_2 t}}{\sigma_1 - \sigma_2}, \quad (2.11)$$

where

$$\sigma_{1,2} = -\frac{bL + RJ}{2JL} \pm \sqrt{\frac{(bL + RJ)^2}{4J^2 L^2} - \frac{bR + K_e K_t}{LJ}} \quad (2.12)$$

are the poles of the transfer functions $H_{V \rightarrow \Omega}(s)$, $H_{V \rightarrow I}(s)$, $H_{\Lambda \rightarrow \Omega}(s)$, and $H_{\Lambda \rightarrow I}(s)$. If, instead, $(bL + RJ)^2 = 4JL(bR + K_e K_t)$, then

$$h(t) = t e^{\sigma t}, \quad (2.13)$$

where

$$\sigma = -\frac{bL + RJ}{2JL} \quad (2.14)$$

is a repeated pole of the transfer functions. It now follows that the angular velocity and current responses to a unit impulse in the driving voltage equal

$$h_{v \rightarrow \omega}(t) = K_t h(t) \quad (2.15)$$

and

$$h_{v \rightarrow i}(t) = b h(t) + J h'(t). \quad (2.16)$$

Similarly, the angular velocity and current responses to a unit impulse in the disturbance torque equal

$$h_{\lambda \rightarrow \omega}(t) = R h(t) + L h'(t) \quad (2.17)$$

and

$$h_{\lambda \rightarrow i}(t) = -K_e h(t). \quad (2.18)$$

Since the poles lie in the left half of the complex plane, the unit-impulse responses decay to 0 exponentially in t and the system is input-to-output stable.

For general $v(t)$ and $\lambda(t)$, the time-dependence of the angular velocity and current are now given by

$$\omega(t) = (K_t L i_0 + J R \omega_0) h(t) + J L \omega_0 h'(t) + (v * h_{v \rightarrow \omega} + \lambda * h_{\lambda \rightarrow \omega})(t) \quad (2.19)$$

and

$$i(t) = (-K_e J \omega_0 + b L i_0) h(t) + J L i_0 h'(t) + (v * h_{v \rightarrow i} + \lambda * h_{\lambda \rightarrow i})(t) \quad (2.20)$$

in terms of the convolution operator $*$.

2.1.2 Steady-state dynamics

The exponential decay of $h(t)$ in Eqs. (2.11) and (2.13) implies that the steady-state responses $\omega_{ss}(t)$ and $i_{ss}(t)$ equal the asymptotic behavior of the convolutions $v * h_{v \rightarrow \omega} + \lambda * h_{\lambda \rightarrow \omega}$ and $v * h_{v \rightarrow i} + \lambda * h_{\lambda \rightarrow i}$, respectively. For example, when $v(t) = V_0 \cos \eta t$ and $\lambda(t) \equiv 0$, we find

$$\omega_{ss}(t) = K_t V_0 \frac{(K_e K_t + b R - J L \eta^2) \cos \eta t + (b L + J R) \eta \sin \eta t}{(b^2 + J^2 \eta^2)(R^2 + L^2 \eta^2) + 2 K_e K_t (b R - J L \eta^2) + K_e^2 K_t^2} \quad (2.21)$$

and

$$i_{ss}(t) = V_0 \frac{(b K_e K_t + b^2 R + J^2 R \eta^2) \cos \eta t + (b^2 L - J K_e K_t + J^2 L \eta^2) \eta \sin \eta t}{(b^2 + J^2 \eta^2)(R^2 + L^2 \eta^2) + 2 K_e K_t (b R - J L \eta^2) + K_e^2 K_t^2}. \quad (2.22)$$

Similarly, when $v(t) \equiv 0$ and $\lambda(t) = \Lambda_0 \cos \eta t$, we find

$$\omega_{ss}(t) = \Lambda_0 \frac{(R K_e K_t + R^2 b + L^2 b \eta^2) \cos \eta t + (R^2 J - L K_e K_t + L^2 J \eta^2) \eta \sin \eta t}{(b^2 + J^2 \eta^2)(R^2 + L^2 \eta^2) + 2 K_e K_t (b R - J L \eta^2) + K_e^2 K_t^2} \quad (2.23)$$

and

$$i_{ss}(t) = -K_e \Lambda_0 \frac{(K_e K_t + b R - J L \eta^2) \cos \eta t + (b L + J R) \eta \sin \eta t}{(b^2 + J^2 \eta^2)(R^2 + L^2 \eta^2) + 2 K_e K_t (b R - J L \eta^2) + K_e^2 K_t^2}. \quad (2.24)$$

To investigate the dependence of the steady-state response on the exci-

tation frequency η , consider the amplitude of the response of the angular velocity to a harmonically varying voltage:

$$\frac{K_t V_0}{\sqrt{(b^2 + J^2 \eta^2)(R^2 + L^2 \eta^2) + 2K_e K_t (bR - JL\eta^2) + K_e^2 K_t^2}}. \quad (2.25)$$

From this expression, we obtain a DC gain of $K_t/(bR + K_e K_t)$. This exceeds 1 if $K_e < 1 - bR/K_t$, and is below 1 otherwise. Furthermore, the amplitude gain approaches 0 asymptotically as η^{-2} when $\eta \rightarrow \infty$. A resonance peak occurs at

$$\eta = \frac{\sqrt{2JLK_e K_t - b^2 L^2 - J^2 R^2}}{\sqrt{2}JL} \quad (2.26)$$

provided that $2JLK_e K_t - b^2 L^2 - J^2 R^2 > 0$. It follows that there exists a unique and transversal crossing of the amplitude gain with the value 1, only if $K_e < 1 - bR/K_t$. If, instead, $K_e > 1 - bR/K_t$, then the amplitude gain equals 1 at two frequencies provided that $2JLK_e K_t - b^2 L^2 - J^2 R^2 > 0$ and the local maximum is bigger than 1, and remains below 1 otherwise.

Similarly, the phase of the steady-state response for the angular velocity is given by

$$-\arctan\left(\frac{(bL + JR)\eta}{K_e K_t + bR - JL\eta^2}\right) \quad (2.27)$$

when $\eta^2 < (K_e K_t + bR)/JL$,

$$\arctan\left(\frac{(bL + JR)\eta}{JL\eta^2 - K_e K_t - bR}\right) - \pi \quad (2.28)$$

when $\eta^2 > (K_e K_t + bR)/JL$, and $-\pi/2$ when $\eta^2 = (K_e K_t + bR)/JL$. It follows that the phase is a continuous decreasing function of η for all η . In particular, the phase lies in the interval $(-\pi, 0]$ for all η .

Consider, instead, the amplitude of the response of the angular velocity to a harmonically varying disturbance torque:

$$\frac{\Lambda_0 \sqrt{R^2 + L^2 \eta^2}}{\sqrt{(b^2 + J^2 \eta^2)(R^2 + L^2 \eta^2) + 2K_e K_t (bR - JL\eta^2) + K_e^2 K_t^2}}. \quad (2.29)$$

From this expression, we obtain a DC gain of $R/(bR + K_e K_t)$. This exceeds 1, provided that $b < 1 - K_e K_t/R$, and is below 1 otherwise. Furthermore, the amplitude gain approaches 0 asymptotically as η^{-1} as $\eta \rightarrow \infty$. A resonance

peak occurs at

$$\eta = \sqrt{\frac{\sqrt{K_e K_t L (K_e K_t L + 2bRL + 2JR^2)} - JR^2}{JL^2}} \quad (2.30)$$

provided that the expression in the outer radical is positive.

2.2 Design Criteria

Now consider assigning the driving voltage to the DC motor in the previous section as the output of an amplifier with gain $(bR + K_e K_t)/K_t$, whose input is the desired angular velocity of the shaft, $\omega_{in}(t)$ (see Fig. 2.2). The open-loop transfer function from ω_{ref} to ω is then given by

$$\tilde{H}_{\Omega_{in} \rightarrow \Omega}(s) := \frac{bR + K_e K_t}{K_t} H_{V \rightarrow \Omega}(s) = \frac{bR + K_e K_t}{(b + Js)(R + Ls) + K_e K_t} \quad (2.31)$$

with a DC gain of 1. Similarly, the open-loop transfer function from ω_{ref} to i is given by

$$\tilde{H}_{\Omega_{in} \rightarrow I}(s) := \frac{bR + K_e K_t}{K_t} H_{V \rightarrow I}(s) = \frac{1}{K_t} \frac{(b + Js)(bR + K_e K_t)}{(b + Js)(R + Ls) + K_e K_t} \quad (2.32)$$

with a DC gain equal to b/K_t .

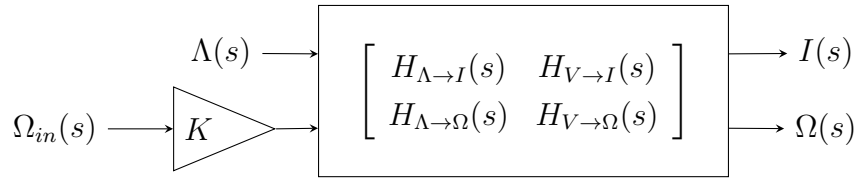


Figure 2.2: System representation of the DC motor with additional input gain. Here, $K = (bR + K_e K_t)/K_t$.

Alternatively, consider assigning the driving voltage to the DC motor as the *sum* of (i) the output of an amplifier with gain $(bR + K_e K_t)/K_t$ whose input is a desired angular velocity of the shaft, $\omega_{in}(t)$, and (ii) the difference between the desired angular velocity of the shaft and its actual angular velocity $\omega(t)$ (see Fig. 2.3).

The corresponding closed-loop transfer function from ω_{in} to ω is then given

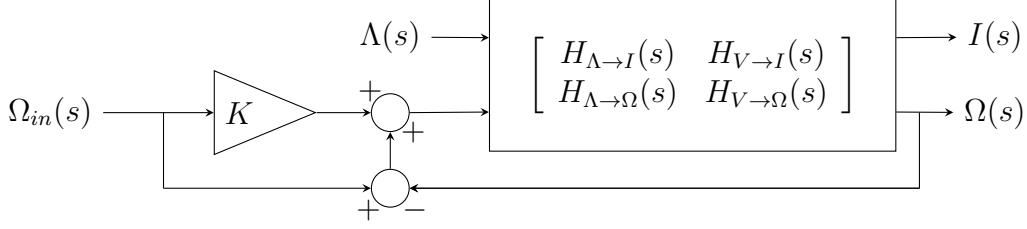


Figure 2.3: System representation of the DC motor with additional input gain and additional feedback.

by

$$\begin{aligned} \hat{H}_{\Omega_{in} \rightarrow \Omega}(s) &:= \frac{bR + K_e K_t + K_t}{K_t} \frac{H_{V \rightarrow \Omega}(s)}{1 + H_{V \rightarrow \Omega}(s)} \\ &= \frac{bR + K_e K_t + K_t}{(b + Js)(R + Ls) + K_e K_t + K_t}, \end{aligned} \quad (2.33)$$

which also has a DC gain of 1. In this case, the closed-loop transfer function from λ to ω is given by

$$\hat{H}_{\Lambda \rightarrow \Omega}(s) := \frac{H_{\Lambda \rightarrow \Omega}(s)}{1 + H_{V \rightarrow \Omega}(s)} = \frac{R + Ls}{(b + Js)(R + Ls) + K_e K_t + K_t}. \quad (2.34)$$

The input-to-output stability of the closed-loop transfer functions $\hat{H}_{\Omega_{in} \rightarrow \Omega}$ and $\hat{H}_{\Lambda \rightarrow \Omega}$ is verified by the observation that their poles again lie in the left half of the complex plane. Alternatively, we may arrive at this conclusion for certain parameter combinations by establishing a positive phase or gain margin for the transfer function $H_{V \rightarrow \Omega}(s)$. These are obtained as the difference between the phase of $H_{V \rightarrow \Omega}(j\eta_1)$ and $-\pi$, where η_1 satisfies $|H_{V \rightarrow \Omega}(j\eta_1)| = 1$, or from the absolute value $|H_{V \rightarrow \Omega}(j\eta_2)|$, where η_2 satisfies $\arg(H_{V \rightarrow \Omega}(j\eta_2)) = -\pi$, respectively. From the discussion above, we recall that the phase lies in $(-\pi, 0]$ for all η and all parameter combinations, again implying stability.

As a further alternative (cf. [18]), consider assigning the driving voltage to the DC motor as the sum of (i) the output of an amplifier with gain $(bR + K_e K_t)/K_t$ whose input is a desired angular velocity of the shaft, $\omega_{in}(t)$, and (ii) the integrated difference between the desired angular velocity of the shaft and its actual angular velocity $\omega(t)$ (see Fig. 2.4).

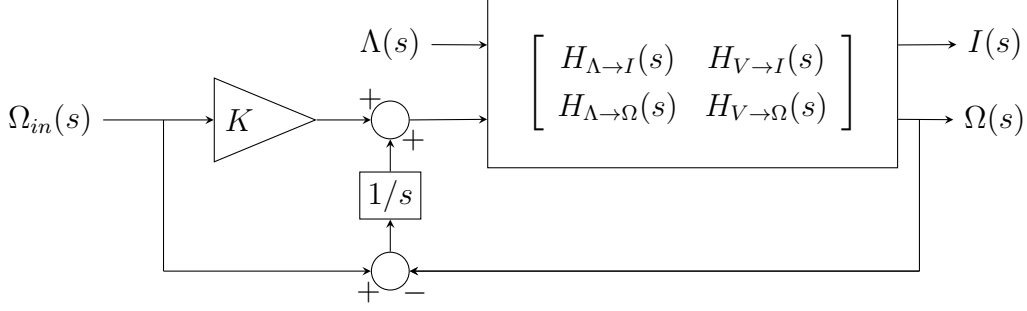


Figure 2.4: System representation of the DC motor with additional input gain and integral feedback.

The corresponding closed-loop transfer function from ω_{ref} to ω is then given by

$$\begin{aligned} \bar{H}_{\Omega_{in} \rightarrow \Omega}(s) &:= \frac{s(bR + K_e K_t) + K_t}{K_t} \frac{H_{V \rightarrow \Omega}(s)}{s + H_{V \rightarrow \Omega}(s)} \\ &= \frac{s(bR + K_e K_t) + K_t}{s(b + Js)(R + Ls) + sK_e K_t + K_t}, \end{aligned} \quad (2.35)$$

which also has a DC gain of 1. In this case, the closed-loop transfer function from λ to ω is given by

$$\begin{aligned} \bar{H}_{\Lambda \rightarrow \Omega}(s) &:= \frac{sH_{\Lambda \rightarrow \Omega}(s)}{s + H_{V \rightarrow \Omega}(s)} \\ &= \frac{s(R + Ls)}{s(b + Js)(R + Ls) + sK_e K_t + K_t}. \end{aligned} \quad (2.36)$$

From the Routh-Hurwitz test [11], it follows that the closed-loop transfer functions $\bar{H}_{\Omega_{in} \rightarrow \Omega}$ and $\bar{H}_{\Lambda \rightarrow \Omega}$ are input-to-output stable provided that $(bR + K_e K_t)(bL + JR) > J L K_t$. The same conclusion follows from the gain margin of $H_{V \rightarrow \Omega}(s)/s$, which here is obtained as

$$-20 \log_{10} \frac{J L K_t}{(bR + K_e K_t)(bL + JR)}. \quad (2.37)$$

A further observation is the disturbance rejection that results for small excitation frequencies from the inclusion of the integrator. Here, the square

of the frequency-dependent gain equals

$$\frac{(R^2 + L^2\eta^2)\eta^2}{(K_t - bL\eta^2)^2 + \eta(K_e K_t - JL\eta^2)^2 + R\eta^2(b(bR + 2K_e K_t) + R(J\eta)^2 - 2JK_t)}. \quad (2.38)$$

It follows that the gain converges to 0 as $\eta \rightarrow 0$ and as η^{-1} as $\eta \rightarrow \infty$. By Descartes' rule [14], there exists a unique global maximum at some positive η .

In general, the phase and gain margins provide a measure of robustness to uncertainty in model parameters, including nonlinear effects. One might want to hold the phase or gain margin fixed while varying model parameters to retain a desired degree of stability, even as the system design is optimized for other criteria.

Consider for example, the system of equations

$$JLK_t - \gamma(bR + K_e K_t)(bL + JR) = 0, \quad (2.39)$$

$$f_\eta(\eta_m, R, K_t; b, L, J, K_e) = 0, \quad (2.40)$$

$$f(\eta_m, R, K_t; b, L, J, K_e) - \mu = 0, \quad (2.41)$$

where $f(\eta, R, K_t; b, L, J, K_e)$ is the expression in Eq. (2.38), the subscript η denotes differentiation with respect to η , and γ and μ correspond to the desired gain margin of $H_{V \rightarrow \Omega}(s)/s$ and maximal amplification of a disturbance torque, respectively. We may consider these equations as determining R , K_t , and η_m as functions of μ for fixed values of γ , b , J , L , and K_e .

Alternatively, we may impose a condition of constant phase margin on the problem of choosing optimal model parameters, as encoded in the following equations

$$|H_{V \rightarrow \Omega}(j\eta_c)| - \eta_c = 0, \quad (2.42)$$

$$\arg(H_{V \rightarrow \Omega}(j\eta_c)) + \frac{\pi}{2} - \varphi = 0, \quad (2.43)$$

$$f_\eta(\eta_m, R, K_t; b, L, J, K_e) = 0, \quad (2.44)$$

$$f(\eta_m, R, K_t; b, L, J, K_e) - \mu = 0. \quad (2.45)$$

Here, the magnitude of $|H_{V \rightarrow \Omega}(j\eta_c)|$ is obtained by substituting η_c for η in Eq. (2.25), $\arg(H_{V \rightarrow \Omega}(j\eta_c))$ is given in Eqs. (2.27-2.28) with the same substitution, and $f(\eta, R, K_t; b, L, J, K_e)$ is again given by the expression in

Eq. (2.38). The variable η_c represents the cross-over frequency for $H_{V \rightarrow \Omega}(s)/s$ and φ is the corresponding phase margin. In this case, the four equations may constitute a system for determining R , K_t , η_m , and η_c as functions of μ for fixed values of φ , b , J , L , and K_e .

A third option is to impose a condition on the minimum distance from the Nyquist plot of the open-loop transfer function $H_{V \rightarrow \Omega}(s)/s$ to the point $(-1, 0)$ in the complex plane. For simplicity, this distance is referred as Nyquist distance through this document. Consider, for example, the equations

$$\left. \frac{d}{d\eta} \left(\frac{\Im(H_{V \rightarrow \Omega}(j\eta))}{\eta} + \frac{1}{2} \frac{|H_{V \rightarrow \Omega}(j\eta)|^2}{\eta^2} \right) \right|_{\eta=\eta_n} = 0, \quad (2.46)$$

$$(\eta_n + \Im(H_{V \rightarrow \Omega}(j\eta_n)))^2 + (\Re(H_{V \rightarrow \Omega}(j\eta_n)))^2 - \delta\eta_n^2 = 0, \quad (2.47)$$

$$f_\eta(\eta_m, R, K_t; b, L, J, K_e) = 0, \quad (2.48)$$

$$f(\eta_m, R, K_t; b, L, J, K_e) - \mu = 0, \quad (2.49)$$

where \Re and \Im denote the real and imaginary parts of the corresponding arguments. Here, η_n represents the frequency at which the tangent vector to the Nyquist curve is perpendicular to the vector from -1 , and δ equals the corresponding squared distance to -1 . As before, these four equations may constitute a system for determining R , K_t , η_m , and η_n as functions of μ for fixed values of δ , b , J , L , and K_e .

2.3 Discussion

In all cases considered in the previous section, given the explicit expression for the transfer function $H_{V \rightarrow \Omega}(s)$, we obtain a system of algebraic and highly nonlinear equations that relate the model parameters, certain characteristic frequencies, and properties of the feedback structure to each other. Due to the complexity of these equations, we must rely on numerical methods for their solution, e.g., Newton's method.

As discussed in chap. 4, we may trace families of solutions by combining nonlinear solvers with manifold covering algorithms. Indeed, with some additional effort, we may achieve this task even in instances where an explicit expression is not available for the open-loop transfer function.

CHAPTER 3

ALGEBRAIC CONTINUATION

In this chapter, we express each of the design problems from Chap. 2 in the form of a restricted continuation problem with a one-dimensional solution manifold. We use COCO [10] to locate a sequence of points on each solution manifold, and consider the implications to the search for optimal values of the design parameters. Through out the remainder of this thesis, we fix $b = 1$, $L = 10$, $J = 0.4$, and $K_e = 1$, and consider variations in the design parameters R and K_t .

3.1 Constant Gain Margin

Consider the first continuation problem defined by Eqs. (2.39-2.41). To represent this problem in canonical form (cf. Eq. (1.1)), denote by $u = (\eta_m, R, K_t)$ the vector of continuation variables, and let

$$\Phi : u \mapsto f_\eta(\eta_m, R, K_t; b, L, J, K_e), \quad (3.1)$$

$$\Psi : u \mapsto \left(\begin{array}{c} \frac{JLK_t}{(bR+K_eK_t)(bL+JR)} \\ f(\eta_m, R, K_t; b, L, J, K_e) \end{array} \right), \quad (3.2)$$

$\kappa = (\gamma, \mu)$, and $\mathbb{I} = \{1\}$. The dimensional deficit of this problem equals 1. It follows that the family of solutions through any regular solution point is a one-dimensional manifold along which the gain margin γ is constant, while the maximum squared amplitude of the steady-state response to a harmonic disturbance torque μ , the design parameters R and K_t , and the extremal frequency η_m vary.

The MATLAB functions `dist_resp`, `gain_margin`, and `dist_resp_deta` below contain COCO-compatible encodings of the zero function and monitor functions, respectively.


```

function [data y] = dist_resp(prob, data, u)
eta_m = u(1);
R      = u(2);
Kt     = u(3);
J      = data.J;
L      = data.L;
b      = data.b;
Ke     = data.Ke;
esq    = eta_m^2;
y      = (L^2*esq + R^2)*esq / ((b^2+J^2*esq)* ...
      (R^2+L^2*esq)*esq-2*Kt*(b*(L-Ke*R)+J* ...
      (R+Ke*L*esq))*esq+Kt^2*(1+Ke^2*esq));
end

```

```

function [data y] = gain_margin(prob, data, u)
R = u(1);
Kt = u(2);
J = data.J;
L = data.L;
b = data.b;
Ke = data.Ke;
y = J*L*Kt / (b*R+Ke*Kt) / (b*L+J*R);
end

```

```

function [data y] = dist_resp_deta(prob, data, u)
eta_m = u(1);
R      = u(2);
Kt     = u(3);
J      = data.J;
L      = data.L;
b      = data.b;
Ke     = data.Ke;
esq    = eta_m^2;
y      = 2*eta_m*(-2*Kt*L*(b*L+J*R)*(L-Ke*R)*esq^2 ...
      -J^2*esq^2*(R^2+L^2*esq)^2 ...
      +Kt^2*(R^2+L^2*esq*(2+Ke^2*esq))) ...
      / ((b^2+J^2*esq)*(R^2+L^2*esq)*esq ...
      -2*Kt*(b*(L-Ke*R) ...
      +J*(R+Ke*L*esq))*esq+Kt^2*(1+Ke^2*esq))^2;
end

```

To initialize the continuation problem, we estimate the values of γ and η_m corresponding to a particular choice of R and K_t . Substitution of $R = 1$ and $K_t = 100$ in the explicit expression for the gain margin gives $\gamma \approx 0.3808$, while a graph of the steady-state voltage amplitude response to a harmonic disturbance torque shows a maximum at $\eta_m \approx 4.9$. Consequently, let $u_0 = (5, 1, 100)$ and suppose that $\gamma = 0.3808$ is the constant value of the gain margin along the corresponding solution manifold.

The following code uses the `coco` entry-point function to perform continuation along this manifold.

```
>> u0 = [5; 1; 100];
>> data = struct('b', 1, 'Ke', 1, 'J', 0.4, 'L', 10);
>> prob = coco_prob();
>> prob = coco_set(prob, 'cont', 'ItMX', 1000, ...
    'h_max', 100, 'NPR', 1, 'h0', 20);
>> prob = coco_set(prob, 'corr', 'TOL', 1.0e-5);
>> prob = coco_add_func(prob, 'phi', @dist_resp_deta, ...
    data, 'zero', 'u0', u0);
>> prob = coco_add_func(prob, 'psi1', @gain_margin, ...
    data, 'inactive', 'gamma', 'uidx', [2;3]);
>> prob = coco_add_func(prob, 'psi2', @dist_resp, data, ...
    'active', 'mu', 'uidx', [1:3]);
>> prob = coco_add_pars(prob, 'pars', [2 3], {'R', 'Kt'}, ...
    'active');
>> prob = coco_set_parival(prob, 'gamma', 0.3808);
>> coco(prob, 'pl_coco', [], 1, {'mu', 'Kt', 'R'}, ...
    {[0 5], [1 300], [0.1 300]});
```

Here, two inactive continuation parameters associated with R and K_t are introduced using the `coco_add_pars` constructor and subsequently released during continuation.

A projection of the solution manifold onto the (μ, R, K_t) coordinate space is shown below in Fig. 3.1. As μ decays monotonically along the manifold, its minimum is attained on the boundary of the computational domain, where $\mu = 2.415$, $R = 1.159$, and $K_t = 300$.

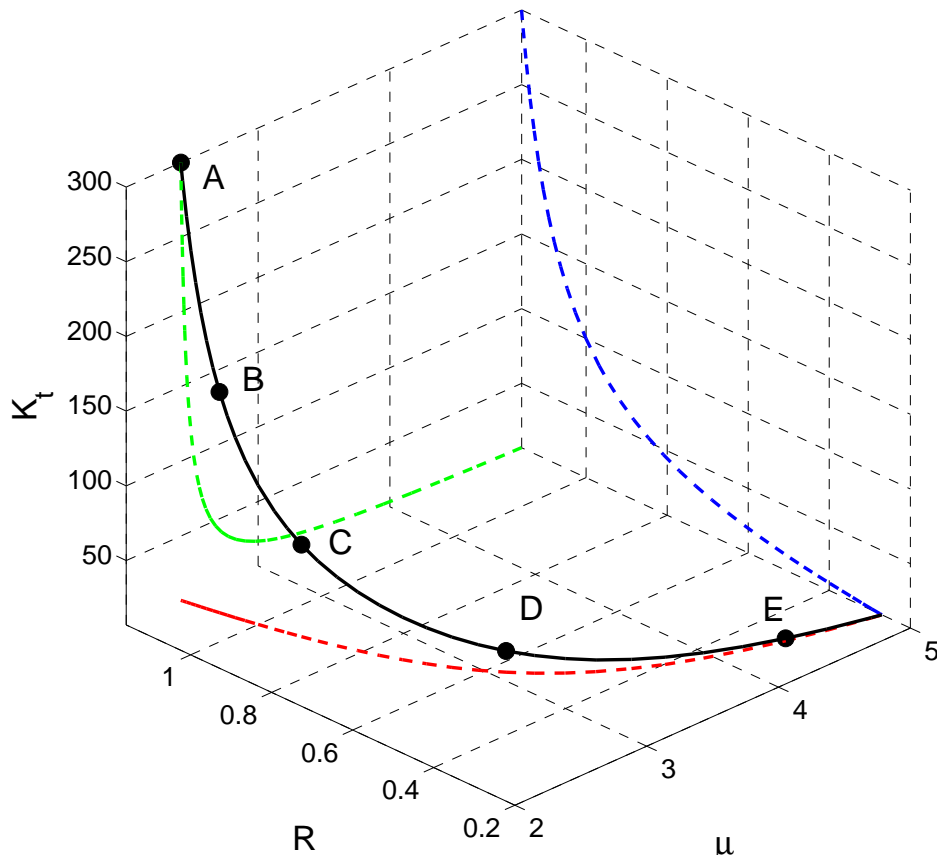


Figure 3.1: Variations in μ , R , and K_t along the one-dimensional manifold obtained for a constant gain margin $\gamma = 0.3808$, and their projections onto the coordinate planes. In this case, the minimal value of μ is attained on the boundary of computational domain.

The Nyquist diagram in Fig. 3.2 collects the graphs of the frequency response functions for several distinct points along the solution manifold. All the Nyquist curves cross the negative imaginary axis at -0.3808 , consistent with the imposition of a constant gain margin. However, as R and K_t decrease, the corresponding Nyquist curve crosses the unit circle further away from the imaginary axis, shows that the phase margin of the corresponding system also decreases.

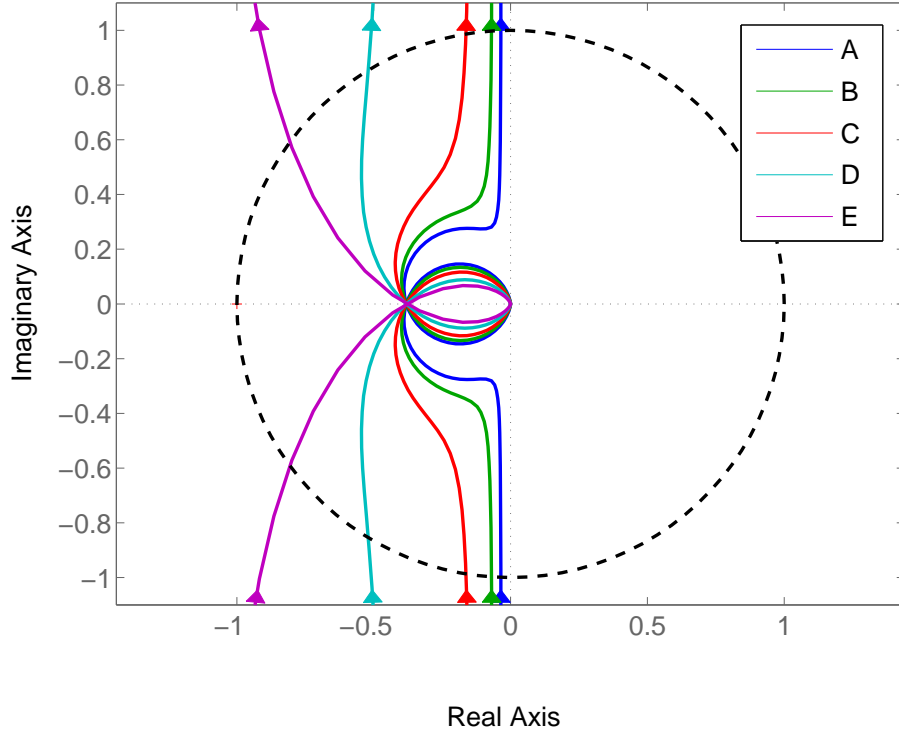


Figure 3.2: The Nyquist curves corresponding to the solution points labeled in Fig. 3.1 cross the negative real axis at the same point.

3.2 Constant Phase Margin

Consider the second continuation problem defined by Eqs. (2.42-2.45). To represent this problem in canonical form, denote by $u = (\eta_m, R, K_t, \eta_c)$ the vector of continuation variables, and let

$$\Phi : u \mapsto \begin{pmatrix} |H_{V \rightarrow \Omega}(j\eta_c)| - \eta_c \\ f_\eta(\eta_m, R, K_t; b, L, J, K_e) \end{pmatrix}, \quad (3.3)$$

$$\Psi : u \mapsto \begin{pmatrix} \arg(H_{V \rightarrow \Omega}(j\eta_c)) \\ f(\eta_m, R, K_t; b, L, J, K_e) \end{pmatrix}, \quad (3.4)$$

$\kappa = (\varphi - \pi/2, \mu)$, and $\mathbb{I} = \{1\}$. The dimensional deficit of this problem equals 1. It follows that the family of solutions through any regular solution point is a one-dimensional manifold along which the phase margin φ is constant, while the maximum squared amplitude of the steady-state response to a harmonic disturbance torque μ , the design parameters R and K_t , the extremal frequency η_m , and the crossover frequency η_c of the open-loop transfer function $H_{V \rightarrow \Omega}(s)/s$ vary.

The MATLAB functions `dist_resp_deta`, `gain_cross`, `phase_margin`, and `dist_resp` contain COCO-compatible encodings of the zero function and monitor functions, respectively. Since `dist_resp_deta` and `dist_resp` are the same as the functions defined for the previous problem, only `gain_cross` and `phase_margin` will be shown below.

```
function [data y] = gain_cross(prob, data, u)
R      = u(1);
Kt     = u(2);
freqc  = u(3);
J      = data.J;
L      = data.L;
b      = data.b;
Ke     = data.Ke;
y      = Kt/sqrt((b^2+J^2*freqc^2)*(R^2+L^2*freqc^2)...
               +2*Ke*Kt*(b*R-J*L*freqc^2)+Ke^2*Kt^2)-freqc;
end
```

```
function [data y] = phase_margin(prob, data, u)
R      = u(1);
Kt     = u(2);
freqc  = u(3);
J      = data.J;
L      = data.L;
b      = data.b;
Ke     = data.Ke;
phsre  = real(Kt/(Ke*Kt+(b+J*freqc*i)*(R+L*freqc*i)));
phsim  = imag(Kt/(Ke*Kt+(b+J*freqc*i)*(R+L*freqc*i)));
y      = atan2(phsim,phsre);
end
```

To initialize the continuation problem, we estimate the values of φ , η_m ,

and η_c corresponding to a particular choice of R and K_t . As before, when $R = 1$ and $K_t = 100$, a graph of the amplitude of the steady-state response to a harmonic disturbance torque shows a maximum at $\eta_m \approx 4.9$. Similarly, graphs of the amplitude and phase of the open-loop frequency-response function $H_{V \rightarrow \Omega}(j\eta)/(j\eta)$ shows that crossover occurs at $\eta_c \approx 1$ with $\varphi \approx 1.461$. Consequently, let $u_0 = (5, 1, 100, 1)$ and suppose that $\varphi = -0.1099 + \pi/2$ is the constant value of the phase margin along the corresponding solution manifold. The following code uses the `coco` entry-point function to perform continuation along this manifold.

```
>> u0 = [5; 1; 100; 1];
>> data = struct('b', 1, 'Ke', 1, 'J', 0.4, 'L', 10);
>> prob = coco_prob();
>> prob = coco_set(prob, 'cont', 'ItMX', 1000, ...
    'h_min', 1e-3, 'h_max', 90, 'NPR', 1, 'h0', 10);
>> prob = coco_add_func(prob, 'phi1', @dist_resp_deta, ...
    data, 'zero', 'u0', u0(1:3));
>> prob = coco_add_func(prob, 'phi2', @gain_cross, ...
    data, 'zero', 'uidx', [2;3], 'u0', u0(4));
>> prob = coco_add_func(prob, 'psil', @phase_margin, data, ...
    'inactive', 'phasemargin', 'uidx', [2:4]);
>> prob = coco_add_func(prob, 'psi2', @dist_resp, data, ...
    'active', 'mu', 'uidx', [1:3]);
>> prob = coco_add_pars(prob, 'pars', [2 3], {'R', 'Kt'}, ...
    'active');
>> prob = coco_set_parival(prob, 'phasemargin', -0.1099);
>> coco(prob, 'p2_coco', [], 1, {'mu' 'R' 'Kt'}, ...
    {[0 5], [1 300], [0.1 300]});
```

A projection of the solution manifold onto the (μ, R, K_t) coordinate space is shown below in Fig. 3.3. Unlike the constant gain margin problem, μ no longer decreases monotonically along the manifold. Within the computational domain, its minimum is attained at a fold point, where $\mu = 0.1459$, $R = 115.1$, and $K_t = 219.4$.

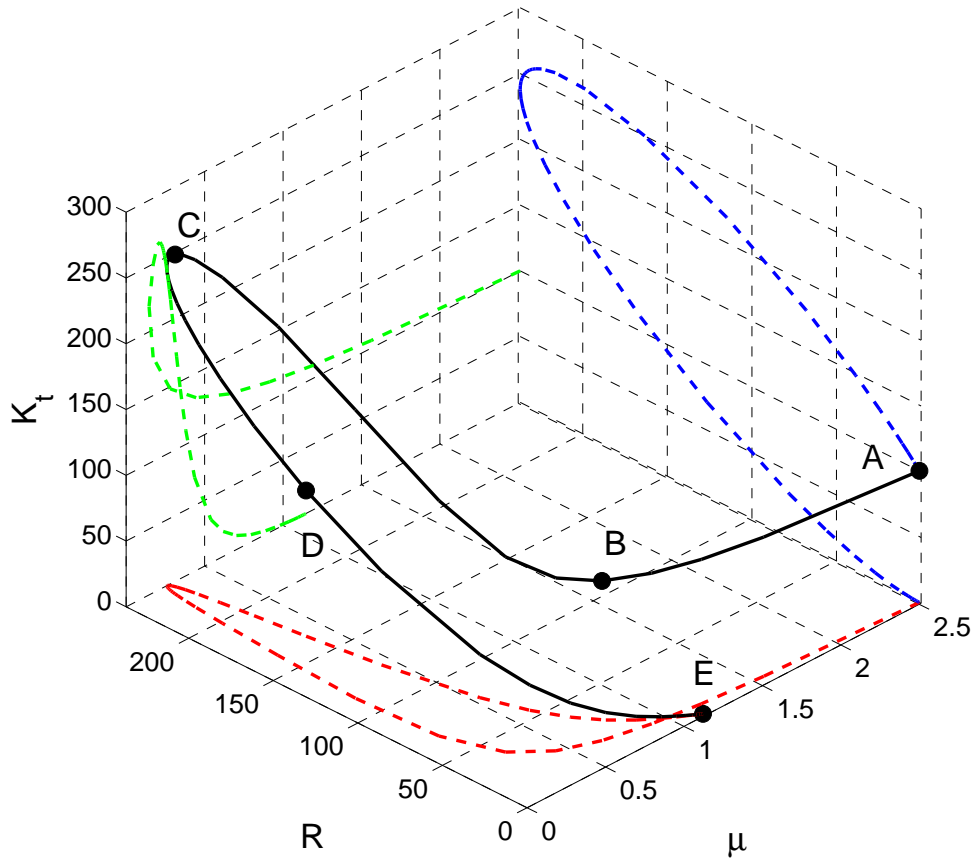


Figure 3.3: Variations in μ , R , and K_t along the one-dimensional manifold obtained for a constant phase margin $\phi = 0.1099$, and their projections onto the coordinate planes. In this case, the minimal value of μ is attained on the interior of the computational domain.

The Nyquist diagram in Figure 3.4 collects the graphs of the frequency response functions for several distinct points along the solution manifold. All the Nyquist curves cross the unit circle at a single point, consistent with the imposition of a constant phase margin. Although the gain margin varies, it remains less than 1 on solution manifold.

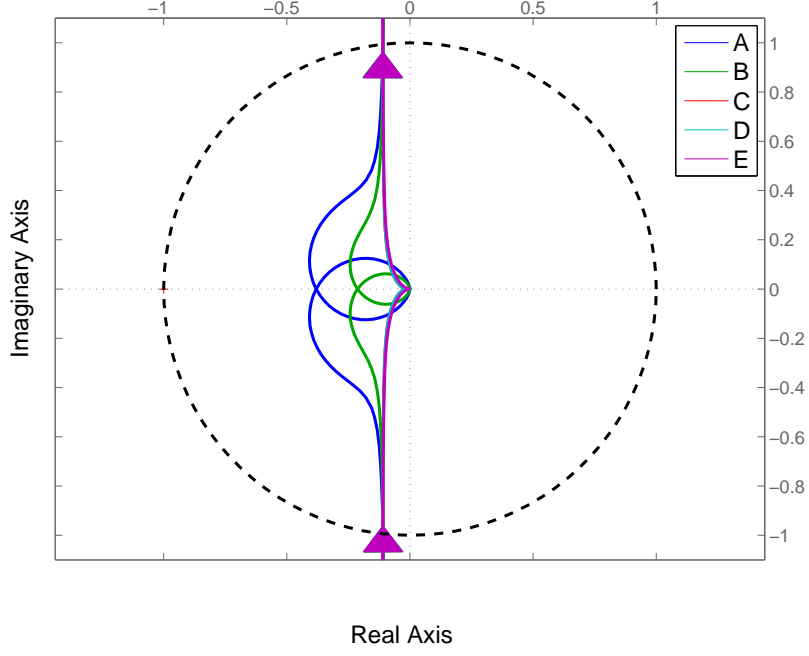


Figure 3.4: The Nyquist curves corresponding to the solution points labeled in Fig. 3.3 cross the unit circle at the same point.

3.3 Constant Nyquist Distance

Consider the third continuation problem Eqs. (2.46-2.49). To represent this problem in canonical form, denote by $u = (\eta_m, R, K_t, \eta_n)$ the vector of continuation variables, and let

$$\Phi : u \mapsto \begin{pmatrix} \frac{d}{d\eta} \left(\frac{\Im(H_{V \rightarrow \Omega}(j\eta))}{\eta} + \frac{1}{2} \frac{|H_{V \rightarrow \Omega}(j\eta)|^2}{\eta^2} \right) \Big|_{\eta=\eta_n} \\ f_\eta(\eta_m, R, K_t; b, L, J, K_e) \end{pmatrix}, \quad (3.5)$$

$$\Psi : u \mapsto \begin{pmatrix} \frac{(\eta_n + \Im(H_{V \rightarrow \Omega}(j\eta_n)))^2 + (\Re(H_{V \rightarrow \Omega}(j\eta_n)))^2}{\eta_n^2} \\ f(\eta_m, R, K_t; b, L, J, K_e) \end{pmatrix}, \quad (3.6)$$

$\kappa = (\delta, \mu)$, and $\mathbb{I} = \{1\}$. The dimensional deficit of this problem equals 1. It follows that the family of solutions through any regular solution point is one-dimensional manifold along which the minimum squared distance δ

from the Nyquist curve of the open-loop transfer function $H_{V \rightarrow \Omega}(s)/s$ to the complex number -1 is constant, while the maximum squared amplitude of the steady-state response to a harmonic disturbance torque μ , the design parameters R and K_t , the extremal frequency η_m , and the critical frequency η_n of the open-loop transfer function corresponding to the minimum distance vary.

The MATLAB functions `dist_resp_deta`, `nyq_dist_deta`, `nyq_dist`, and `dist_resp` contain COCO-compatible encodings of the zero function and monitor functions, respectively. Since `dist_resp_deta` and `dist_resp` are the same as the functions defined for the previous problem, we only show `nyq_dist_deta` and `nyq_dist` below.

```
function [data y] = nyq_dist_deta(prob, data, u)
R      = u(1);
Kt     = u(2);
freqc  = u(3);
b      = data.b;
J      = data.J;
L      = data.L;
Ke     = data.Ke;
y      = -((Kt*(Ke^2*Kt^3-2*b^3*L^3*freqc^4-...
            2*b*J^2*L*freqc^4*(R^2+2*L^2*freqc^2)+...
            J^2*freqc^2*(2*Kt*R^2+3*Kt*L^2*freqc^2-...
            2*J*R^3*freqc^2-4*J*L^2*R*freqc^4)+...
            b^2*(Kt*R^2+2*Kt*L^2*freqc^2-2*J*L^2*R*freqc^4)+...
            2*Ke*Kt*(2*J*L*freqc^2*(-Kt+J*R*freqc^2)+...
            b*(Kt*R+2*J*L^2*freqc^4))))/(freqc^3*(Ke^2*Kt^2+...
            2*Ke*Kt*(b*R-J*L*freqc^2)+...
            (b^2+J^2*freqc^2)*(R^2+L^2 *freqc^2))^2));
end
```

```
function [data y] = nyq_dist(prob, data, u)
R      = u(1);
Kt     = u(2);
freqc  = u(3);
J      = data.J;
L      = data.L;
b      = data.b;
Ke     = data.Ke;
```

```

y      = (Kt^2*(1+Ke^2*freqc^2)+...
          freqc^2*(b^2+J^2*freqc^2)*(R^2+L^2*freqc^2)...
          -2*Kt*freqc^2*(b*(L-Ke*R)+J*(R+Ke*L*freqc^2)))/...
          (freqc^2*(Ke^2*Kt^2+2*Ke*Kt*(b*R-J*L*freqc^2)+...
          (b^2+J^2*freqc^2)*(R^2+L^2*freqc^2)));
end

```

To initialize the continuation problem, we estimate the values of δ , η_m , and η_n corresponding to a particular choice of R and K_t . As before, when $R = 1$ and $K_t = 100$, a graph of the amplitude of the steady-state response to a harmonic disturbance torque shows a maximum at $\eta_m \approx 4.9$. Similarly, the Nyquist diagram of the open-loop frequency-response function $H_{V \rightarrow \Omega}(j\eta)/(j\eta)$ shows that the minimum distance to -1 occurs at $\eta_n \approx 4.8$ with $\delta \approx 0.36$. Consequently, let $u_0 = (5, 1, 100, 5)$ and suppose that $\delta = 0.36$ is the constant value of the locally minimal squared distance along the corresponding solution manifold. The following code uses the `coco` entry-point function to perform continuation along this manifold.

```

>> u0=[5; 1; 100; 5];
>> data = struct('b', 1, 'Ke', 1, 'J', 0.4, 'L', 10);
>> prob = coco_prob();
>> prob = coco_set(prob, 'corr', 'ItMX', 20);
>> prob = coco_set(prob, 'cont', 'ItMX', 1000, ...
                  'h_min', 1e-2, 'h_max', 90, 'NPR', 1, 'h0', 10);
>> prob = coco_add_func(prob, 'phi1', @dist_resp_deta, ...
                      data, 'zero', 'u0', u0(1:3));
>> prob = coco_add_func(prob, 'phi2', @nyq_dist_deta, ...
                      data, 'zero', 'uidx', [2;3], 'u0', u0(4));
>> prob = coco_add_func(prob, 'psi1', @nyq_dist, data, ...
                      'inactive', 'delta', 'uidx', [2:4]);
>> prob = coco_add_func(prob, 'psi2', @dist_resp, data, ...
                      'active', 'mu', 'uidx', [1:3]);
>> prob = coco_add_pars(prob, 'pars', [2 3], {'R', 'Kt'});
>> prob = coco_set_parival(prob, 'delta', 0.36);
>> coco(prob, 'P3_COCO', [], 1, {'mu' 'Kt' 'R'}, ...
        {[0 5], [1 300], [0.1 300]});

```

A projection of the solution manifold onto the (μ, R, K_t) coordinate space is shown below in Fig. 3.5. Unlike the constant gain margin problem, μ no longer decreases monotonically along the manifold. Within the computational domain, its minimum is again attained at a fold point, where $\mu = 1.881$,

$R = 7.481$, and $K_t = 3.559$.

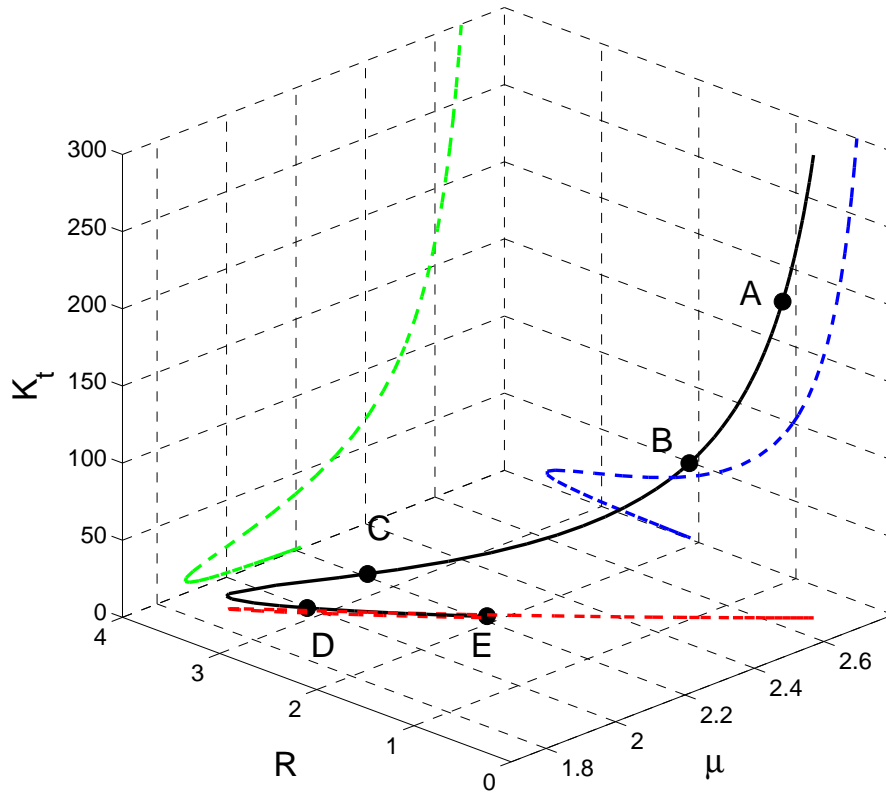


Figure 3.5: Variations in μ , R , and K_t along the one-dimensional manifold obtained for a constant locally minimal squared distance $\delta = 0.36$ from the Nyquist curve to -1 , and their projections onto the coordinate planes. In this case, the minimal value of μ is attained on the interior of the computational domain.

The Nyquist diagram in Fig. 3.6 collects the graphs of the frequency response functions for several distinct points along the solution manifold. All the Nyquist curves are tangential to the circle centered on -1 with radius 0.6 , consistent with the imposition of a constant distance to -1 .

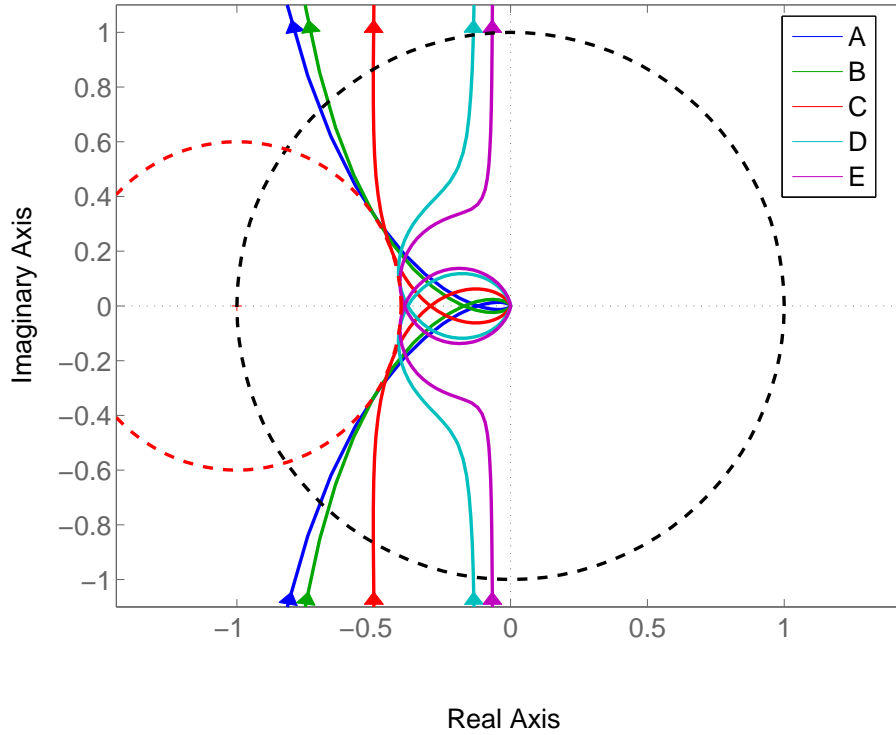


Figure 3.6: The Nyquist curves corresponding to solution points labeled in Fig. 3.5 have the same Nyquist distance to -1 . The red dashed circle represents the circle has a radius of 0.6.

3.4 Discussion

The results in this chapter show that it is possible to design for improved disturbance rejection while imposing constraints on the system stability. The three stability criteria introduced in the previous chapter correspond to three different families of solution manifolds. Depending on the criteria, the optimal solution may be attained either on the boundary or in the interior of the computational domain.

As an alternative, denote by $u = (\eta_m, \eta_{c,1}, \eta_{c,2}, R, K_t)$ the vector of contin-

uation variables, and let

$$\Phi : u \mapsto \begin{pmatrix} |H_{V \rightarrow \Omega}(j\eta_{c,1})| - \eta_{c,1} \\ \arg(H_{V \rightarrow \Omega}(j\eta_{c,2})) + \frac{\pi}{2} \\ f_\eta(\eta_m, R, K_t; b, L, J, K_e) \end{pmatrix}, \quad (3.7)$$

$$\Psi : u \mapsto \begin{pmatrix} \arg(H_{V \rightarrow \Omega}(j\eta_{c,1})) \\ |H_{V \rightarrow \Omega}(j\eta_{c,2})| / \eta_{c,2} \\ f(\eta_m, R, K_t; b, L, J, K_e) \end{pmatrix}, \quad (3.8)$$

and $\mathbb{I} = \emptyset$. The dimensional deficit of this problem equals 2. It follows that the family of solutions through any regular solution point is a two-dimensional manifold along which the gain margin, the phase margin, and the maximum squared amplitude of the steady-state response to a harmonic disturbance torque vary. This formulation can be used for multi-objective optimization.

In the next chapter, we use control based continuation to repeat the analysis in this chapter without assuming explicit knowledge of the system model.

CHAPTER 4

CONTROL-BASED CONTINUATION

In this chapter, we replace explicit model of the DC motor in the continuation analysis with simulated experiments and corresponding measurements. The continuation problems considered in the previous chapter are composed of conditions in terms of an open-loop and a closed-loop system respectively. Here, we use control-based continuation to analyze each system separately, and show how such systems can be coupled experimentally in order to again perform design optimization.

4.1 Elementary Experiments

Consider the block diagram shown in Fig. 4.1. The corresponding transfer function $H_{V \rightarrow \Theta}(s) = H_{V \rightarrow \Omega}(s)/s$ is the open-loop transfer function analyzed in previous chapters. If we have an explicit expression for the transfer function $H_{V \rightarrow \Omega}$, then we can determine the frequency-response function associated with steady-state responses of $\theta(t)$ to harmonic inputs $v(t) = \cos \eta t$, as was done in Chap. 2. This could then be used to impose additional conditions on the steady-state response in the form of algebraic equations. In contrast, if the system is treated as a black box, then the frequency-response function can be found only through experiments.

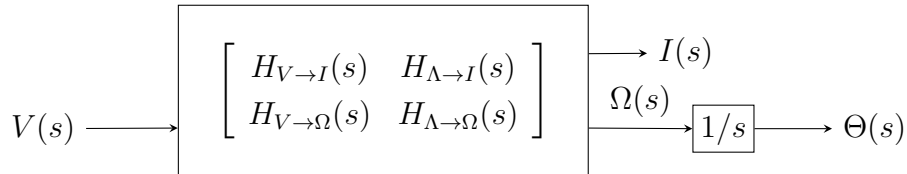


Figure 4.1: Open-loop system representation of the DC motor without disturbance torque and with additional integrator in the output.

In such an experiment, a measurement of the response amplitude or phase

would be made after sufficient convergence to the steady-state solution. We can modify the rate of convergence through the imposition of feedback, as suggested in Fig. 4.2, in terms of the reference signals I_{ref} , Ω_{ref} , and Θ_{ref} . The transfer functions C_I , C_Ω , and C_Θ determine the locations of the poles, and can be designed so that the system is input-output stable and a desired settling time is achieved. Here, we assume proportional control and replace the transfer functions by the corresponding gains K_I , K_Ω , and K_Θ . In this case,

$$\Theta = \frac{H_{V \rightarrow \Omega}(V + K_I I_{ref} + K_\Omega \Omega_{ref} + K_\Theta \Theta_{ref})}{s + (K_\Omega s + K_\Theta)H_{V \rightarrow \Omega} + K_I s H_{V \rightarrow I}}, \quad (4.1)$$

$$\Omega = \frac{s H_{V \rightarrow \Omega}(V + K_I I_{ref} + K_\Omega \Omega_{ref} + K_\Theta \Theta_{ref})}{s + (K_\Omega s + K_\Theta)H_{V \rightarrow \Omega} + K_I s H_{V \rightarrow I}}, \quad (4.2)$$

$$I = \frac{s H_{V \rightarrow I}(V + K_I I_{ref} + K_\Omega \Omega_{ref} + K_\Theta \Theta_{ref})}{s + (K_\Omega s + K_\Theta)H_{V \rightarrow \Omega} + K_I s H_{V \rightarrow I}}. \quad (4.3)$$

Here, the poles are the roots of the polynomial

$$JLs^3 + (K_I J + bL + JR)s^2 + (bK_I + K_t K_\Omega + K_e K_t + bR)s + K_t K_\Theta. \quad (4.4)$$

By Routh-Hurwitz Stability Criterion, the system is therefore asymptotically stable if

$$(bK_I + K_t K_\Omega + K_e K_t + bR)(K_I J + bL + JR) > J L K_t K_\Theta. \quad (4.5)$$

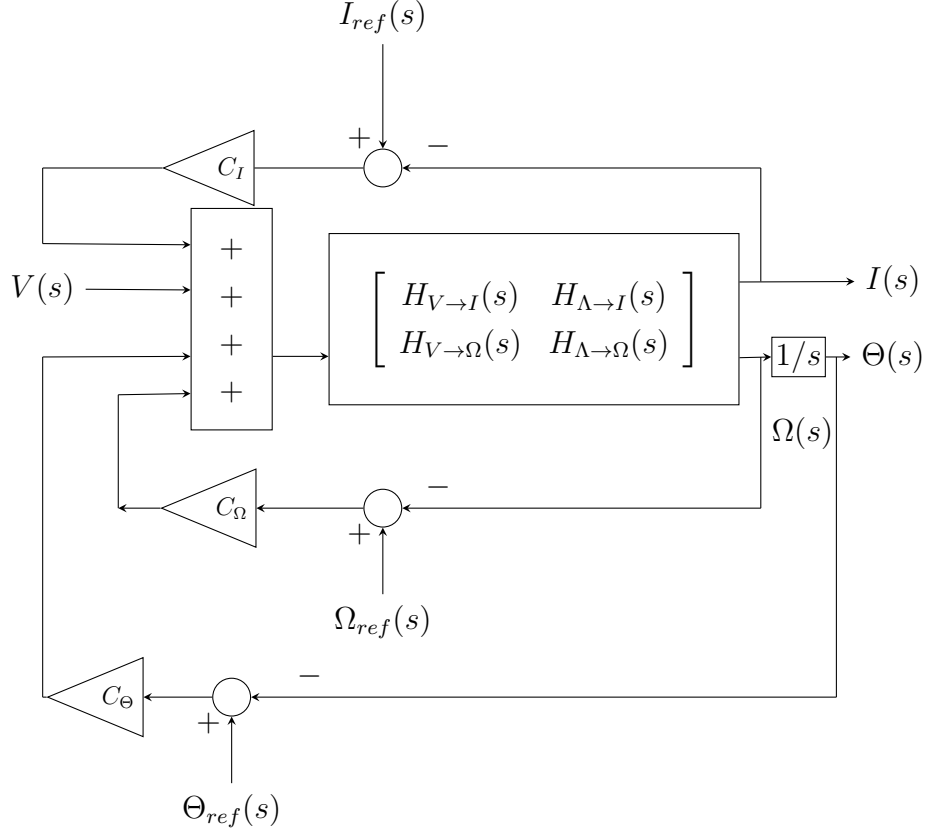


Figure 4.2: System representation of the DC motor without disturbance torque and with additional integrator in the output and additional reference feedback.

By construction, the steady-state responses to a harmonic input $v(t) = \cos \eta t$ are identical to those in the absence of feedback, provided that the reference signals $i_{ref}(t)$, $\omega_{ref}(t)$, and $\theta_{ref}(t)$ equal these steady-state responses. In practice, suppose that $i_{ref}(t) = \alpha_i \cos \eta t + \beta_i \sin \eta t$, $\omega_{ref}(t) = \alpha_\omega \cos \eta t + \beta_\omega \sin \eta t$, and $\theta_{ref}(t) = \alpha_\theta \cos \eta t + \beta_\theta \sin \eta t$, and let the signals $A_i \cos \eta t + B_i \sin \eta t$, $A_\omega \cos \eta t + B_\omega \sin \eta t$, and $A_\theta \cos \eta t + B_\theta \sin \eta t$ denote the corresponding steady-state responses for $i(t)$, $\omega(t)$, and $\theta(t)$. Notably, each of the upper-case coefficients depend on all the lower-case coefficients, the excitation frequency, and the system parameters. A non-invasive feedback structure [32]

then results provided that

$$\begin{pmatrix} A_i - \alpha_i \\ A_\omega - \alpha_\omega \\ A_\theta - \alpha_\theta \\ B_i - \beta_i \\ B_\omega - \beta_\omega \\ B_\theta - \beta_\theta \end{pmatrix} = 0. \quad (4.6)$$

We can embed these equations with a continuation problem that requires imposition of constraints on the steady-state response.

Analogously, consider the block diagram shown below in Fig. 4.3. The corresponding transfer function $sH_{\Lambda \rightarrow \Omega}(s)/(s + H_{V \rightarrow \Omega}(s))$ describes the angular velocity response to a disturbance torque discussed in Chap. 2. As before, if the system is treated as a black box, then the corresponding frequency-response function can be found only through experiments.

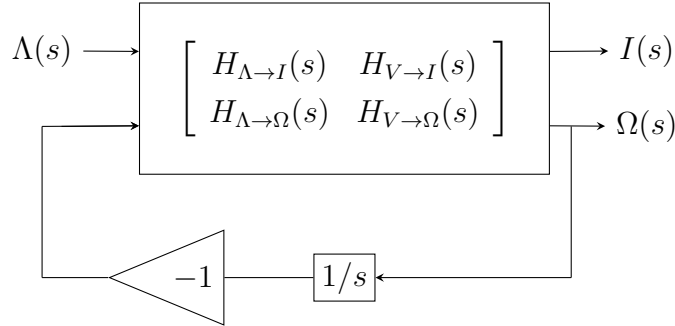


Figure 4.3: Closed-loop system representation of the DC motor with negative integral feedback.

To this end, consider the imposition of feedback, as suggested in Fig. 4.4, in terms of the reference signals I_{ref} , Ω_{ref} , and Θ_{ref} and the proportional gains K_I , K_Ω , and K_Θ . In this case, The solution to the above equations is

$$\Omega = \frac{sH_{\Lambda \rightarrow \Omega}(\Lambda + K_I I_{ref} + K_\Omega \Omega_{ref} + K_\Theta \Theta_{ref})}{(s + H_{V \rightarrow \Omega})(1 + H_{\Lambda \rightarrow I} K_I) - H_{\Lambda \rightarrow \Omega}(H_{V \rightarrow I} K_I - K_\Omega s)}, \quad (4.7)$$

$$I = \frac{(H_{\Lambda \rightarrow I} H_{V \rightarrow \Omega} - H_{V \rightarrow I} H_{\Lambda \rightarrow \Omega} + H_{\Lambda \rightarrow I} s)(\Lambda + K_I I_{ref} + K_\Omega \Omega_{ref} + K_\Theta \Theta_{ref})}{(s + H_{V \rightarrow \Omega})(1 + H_{\Lambda \rightarrow I} K_I) - H_{\Lambda \rightarrow \Omega}(H_{V \rightarrow I} K_I - K_\Omega s)}. \quad (4.8)$$

Here, the poles are the roots of the polynomial

$$JLs^3 + (K_\Omega L + bL + JR)s^2 + (K_e(K_t - K_I) + K_\Theta L + (b + K_\Omega)R)s + K_t + K_\Theta R - K_\Omega. \quad (4.9)$$

By Routh-Hurwitz Stability Criterion, the system is therefore stable if

$$K_e(K_t - K_I)(Lb + LK_\Omega + JR) + JL(K_\Omega - K_t) + \Sigma > 0, \quad (4.10)$$

$$K_t + K_\Theta R - K_\Omega > 0, \quad (4.11)$$

where $\Sigma = (b + K_\Omega)(L^2 K_\Theta + JR^2 + LR(b + K_\Omega))$.

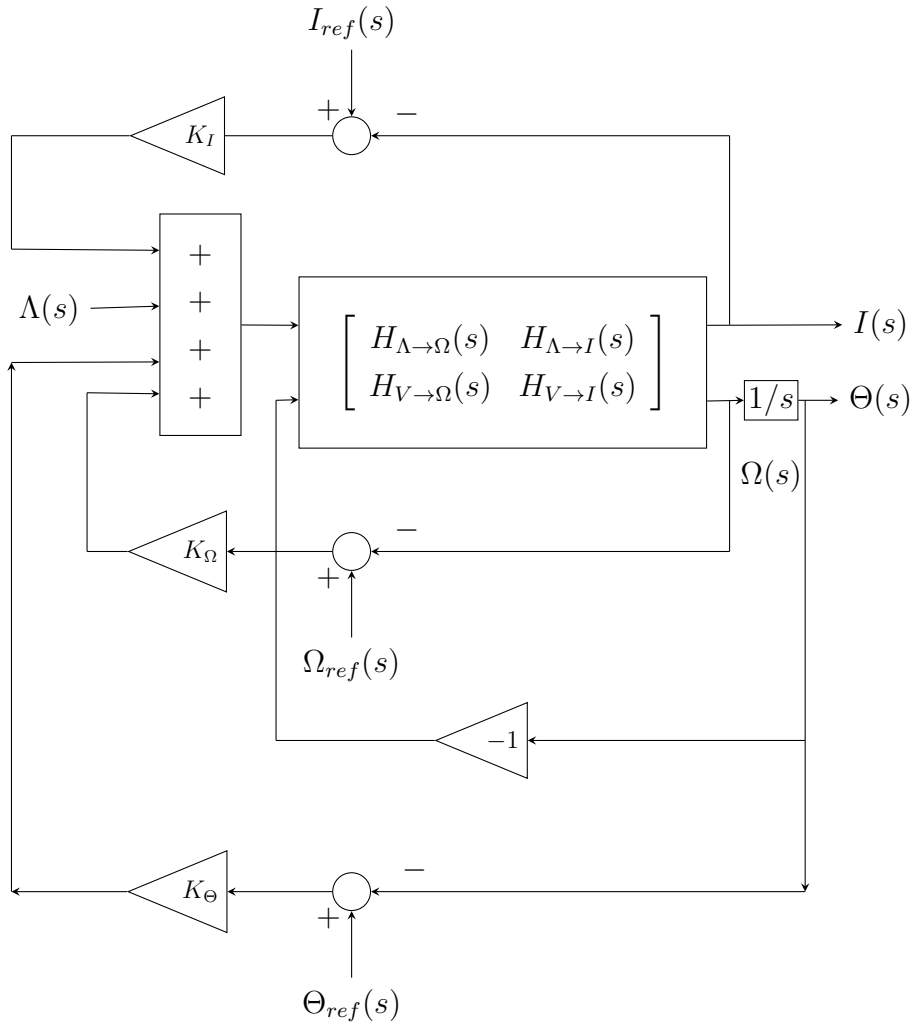


Figure 4.4: System representation of the DC motor with additional negative integral feedback and reference feedback.

By construction, the steady-state responses to a harmonic input $\lambda(t) =$

$\cos \eta t$ are identical to those of the problem in the absence of feedback, provided that the reference signals $i_{ref}(t)$, $\omega_{ref}(t)$, and $\theta_{ref}(t)$ equal these steady-state responses. In practice, suppose that $i_{ref}(t) = \alpha_i \cos \eta t + \beta_i \sin \eta t$, $\omega_{ref}(t) = \alpha_\omega \cos \eta t + \beta_\omega \sin \eta t$, and $\theta_{ref}(t) = \alpha_\theta \cos \eta t + \beta_\theta \sin \eta t$, and let the signals $A_i \cos \eta t + B_i \sin \eta t$, $A_\omega \cos \eta t + B_\omega \sin \eta t$, and $A_\theta \cos \eta t + B_\theta \sin \eta t$ denote the corresponding steady-state responses for $i(t)$, $\omega(t)$, and $\theta(t)$. As before, each of the upper-case coefficients depend on all the lower-case coefficients, the excitation frequency, and the system parameters. A non-invasive feedback structure then results provided that

$$\begin{pmatrix} A_i - \alpha_i \\ A_\omega - \alpha_\omega \\ A_\theta - \alpha_\theta \\ B_i - \beta_i \\ B_\omega - \beta_\omega \\ B_\theta - \beta_\theta \end{pmatrix} = 0. \quad (4.12)$$

We can embed these equations with a continuation problem that requires imposition of constraints on the steady-state response.

4.2 Frequency Sweeps

Consider the SIMULINK implementation shown in Fig. 4.5 of the feedback structure in Fig. 4.2. As suggested above, each reference signal is of the form $\alpha \cos \eta t + \beta \sin \eta t$. Simulation for some fixed integration time, sufficient in duration to allow transients to settle, followed by identification of the coefficients in the decomposition $A \cos \eta t + B \sin \eta t$ of each of the steady-state responses then allows evaluation of the left-hand side of Eq. (4.6).

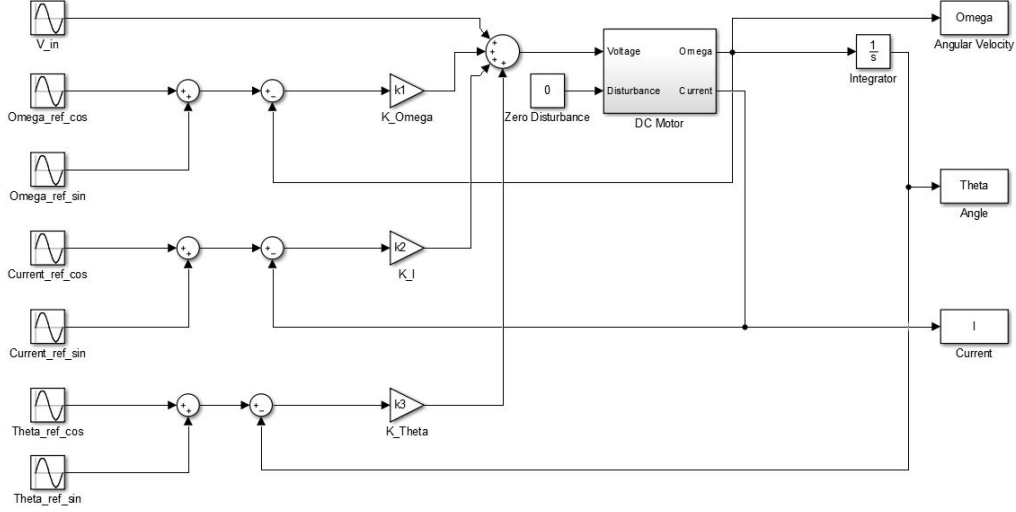


Figure 4.5: SIMULINK realization of Fig. 4.2

Let $u = (\eta, R, K_t, \alpha_\omega, \beta_\omega, \alpha_i, \beta_i, \alpha_\theta, \beta_\theta, \phi)$ be a vector of continuation variables, and consider the restricted continuation problem defined by

$$\Phi : u \mapsto \begin{pmatrix} A_i - \alpha_i \\ A_\omega - \alpha_\omega \\ A_\theta - \alpha_\theta \\ B_i - \beta_i \\ B_\omega - \beta_\omega \\ B_\theta - \beta_\theta \\ \beta_\theta \cos \phi - \alpha_\theta \sin \phi \end{pmatrix}, \quad (4.13)$$

$$\Psi : u \mapsto \begin{pmatrix} \eta \\ \alpha_\theta^2 + \beta_\theta^2 \\ R \\ K_t \\ \phi \end{pmatrix}, \quad (4.14)$$

and $\mathbb{I} = \{3, 4\}$. The dimensional deficit of this problem equals 1. It follows that the family of solutions through any regular solution point is one-dimensional manifold. This manifold is parameterized by η . Each point corresponds to a unique set of trigonometric coefficients for the steady-state responses and phase ϕ of $\theta(t)$ resulting from the input $v(t) = \cos \eta t$. The corresponding value of the second continuation parameter is the squared am-

plitude of $\theta(t)$.

The MATLAB functions `openloopssystem` and `amplitude` below contain COCO-compatible encodings of the zero functions and the squared amplitude monitor function, respectively.

```
function [data y] = openloopssystem(prob, data, u)
k1      = data.ok1;
k2      = data.ok2;
k3      = data.ok3;
omega0  = data.ox0(1);
current0 = data.ox0(2);
theta0  = data.ox0(3);
b       = data.b;
J       = data.J;
L       = data.L;
Ke      = data.Ke;
eta     = u(1);
R       = u(2);
Kt      = u(3);
v2r     = u(4);
v2i     = u(5);
v3r     = u(6);
v3i     = u(7);
v4r     = u(8);
v4i     = u(9);
th      = u(10);
T       = 2*pi/eta;
tstart  = 0;
tsam    = 20*T;
tstep   = T/4;
simout  = sim('simopenloopssystem', 'SrcWorkspace', ...
             'current');
omega   = simout.get('omega');
current = simout.get('current');
theta   = simout.get('theta');
data.ox0 = [omega(end); current(end); theta(end)];
tsize   = numel(theta);
fomega  = fft(omega(tsize-4:tsize-1)); %4pts
y       = [v2r-real(fomega(2))/2; v2i-imag(fomega(2))/2];
fcurrent = fft(current(tsize-4:tsize-1)); %4pts
y       = [y; v3r-real(fcurrent(2))/2; ...
```

```

        v3i-imag(fcurrent(2))/2];
ftheta = fft(theta(tsize-4:tsize-1)); %4pts
y       = [y; v4r-real(ftheta(2))/2; ...
          v4i-imag(ftheta(2))/2; ...
          v4i*cos(th)-v4r*sin(th)];
end

function [data y] = amplitude(prob, data, u)
v4r = u(1);
v4i = u(2);
y   = v4r^2+v4i^2;
end

```

Here, `simopenloopssystem` refers to the SIMULINK model of the open-loop system (see Fig. 4.5). The MATLAB `fft` function is used to find the coefficient amplitudes for each steady-state response. Since we know that the response is harmonic, it suffices to sample four evenly distributed points over one period.

To initialize the continuation problem, let u_0 correspond to the steady-state response obtained from harmonic excitation at $\eta = 5$ with $R = 1$ and $K_t = 100$. The following code uses the `coco` entry-point function to perform continuation along the associated one-dimensional solutions manifold.

```

>> data = struct('k1', 10, 'k2', 10, 'k3', 10, 'b', 1, ...
                'J', 0.4, 'L', 10, 'Ke', 1, 'x0', [0; 0; 0]);
>> u0   = [5; 1; 100; 0.037; -1.9; 0.039; -0.018; ...
          -0.38; -0.0074; -3.1221];
>> prob = coco_prob();
>> prob = coco_set(prob, 'cont', 'PtMX', 1000, ...
                  'h0', 1, 'h_max', 50, 'al_max', 10, ...
                  'NPR', 1);
>> prob = coco_set(prob, 'corr', 'TOL', 1.0e-5);
>> prob = coco_add_func(prob, 'plinit_o_phil', ...
                       @openloopssystem, data, 'zero', 'u0', u0);
>> prob = coco_add_func(prob, 'plinit_o_psil', ...
                       @amplitude, data, 'active', ...
                       'sqmag', 'uidx', [8 9]);
>> prob = coco_add_pars(prob, 'pars', [1 2 3 10], ...
                       {'eta', 'R', 'Kt', 'o_phs'});
>> prob = coco_add_event(prob, 'co', 'o_phs', -pi);

```

```

>> bd_phsco = coco(prob, 'plinit_o_gmdetect', [], ...
    1, {'eta' 'sqmag' 'o_phs'}, [4 6]);
>> lab_phsco = coco_bd_labs(bd_phsco, 'co');
>> chart_phsco = coco_read_solution('', 'gmdetect', ...
    lab_phsco(end), 'chart');

```

A projection of the solution manifold onto the (η, ϕ) coordinate plane is shown below in Fig. 4.6. The phase crosses $-\pi$ when $\eta = 5.025$. The squared amplitude of $\theta(t)$ at this point is 0.145, corresponding to a gain margin of 0.3808 (cf. the initialization in Chap. 3 of γ).

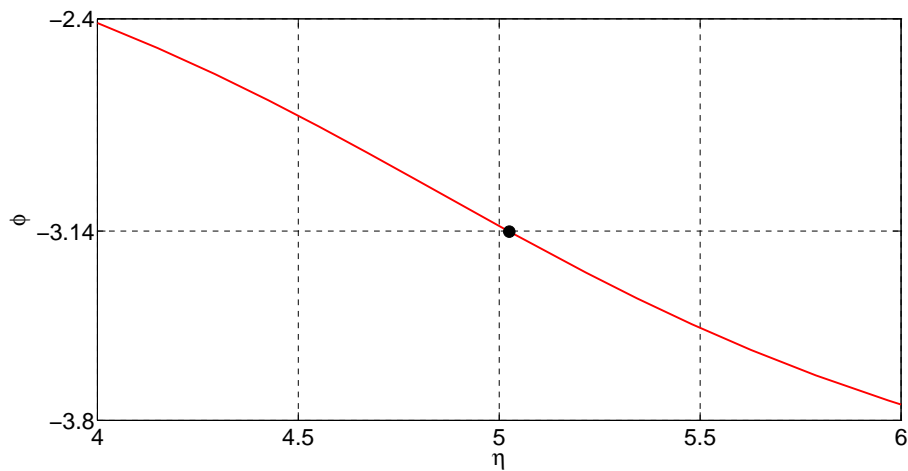


Figure 4.6: Phase of the frequency response function $H_{V \rightarrow \Omega}(j\eta)/\eta$. Here, the black dot corresponds to the phase crossover frequency.

The same initialization can be applied to the constant phase margin problem by changing the detected event from phase crossover to gain crossover [1], as shown in the following code.

```

>> data = struct('k1', 10, 'k2', 10, 'k3', 10, 'b', 1, ...
    'J', 0.4, 'L', 10, 'Ke', 1, 'x0', [0; 0; 0]);
>> u0 = [5; 1; 100; 0.037; -1.9; 0.039; -0.018; ...
    -0.38; -0.0074; -3.1221];
>> prob = coco_prob();
>> prob = coco_set(prob, 'cont', 'PtMX', 1000, ...
    'h0', 1, 'h_max', 50, 'al_max', 10, ...
    'NPR', 1);
>> prob = coco_set(prob, 'corr', 'TOL', 1.0e-5);

```

```

>> prob = coco_add_func(prob, 'plinit_o_phi1', ...
@openloopssystem, data, 'zero', 'u0', u0);
>> prob = coco_add_func(prob, 'plinit_o_psi1', ...
@amplitude, data, 'active', ...
'sqmag', 'uidx', [8 9]);
>> prob = coco_add_pars(prob, 'pars', [1 2 3 10], ...
{'eta', 'R', 'Kt', 'o_phs'});
>> prob = coco_addevent(prob, 'co', 'sqmag', 1);
>> bd_magco = coco(prob, 'pmdetect', [], 1, ...
{'eta' 'sqmag' 'phase'}, [1 5.1]);
>> lab_magco = coco_bd_labs(bd_magco, 'co');
>> chart_magco = coco_read_solution('', 'pmdetect', ...
lab_magco(end), 'chart');

```

A projection of the solution manifold onto the (η, γ) coordinate plane is shown below in Fig. 4.7. The phase shift at the gain crossover frequency is -1.68071 , which corresponds to the phase margin $\varphi = -0.1099 + \pi/2$ (cf. the initialization in Chap. 3 of φ).

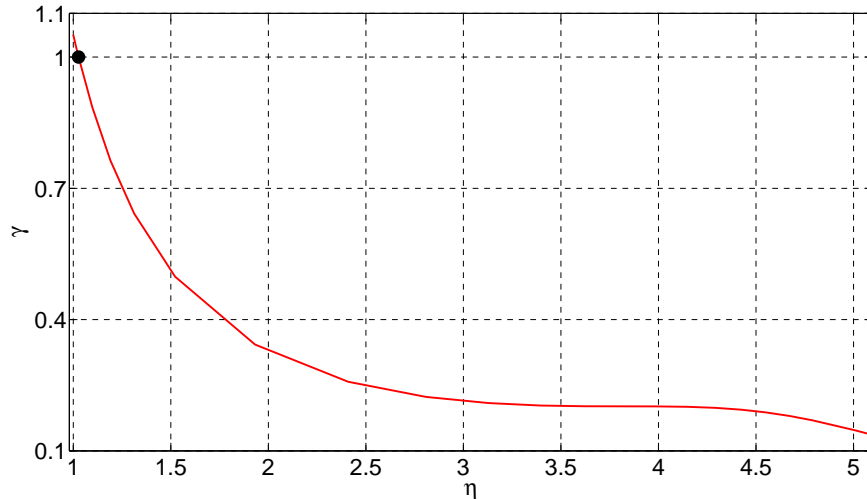


Figure 4.7: Magnitude of the frequency response function $H_{V \rightarrow \Omega}(j\eta)/\eta$. Here, the black dot corresponds to the gain crossover frequency.

Next, let $u = (\eta_1, R_1, K_{t,1}, \alpha_{\omega,1}, \beta_{\omega,1}, \alpha_{i,1}, \beta_{i,1}, \alpha_{\theta,1}, \beta_{\theta,1}, \eta_2, R_2, K_{t,2}, \alpha_{\omega,2}, \beta_{\omega,2}, \alpha_{i,2}, \beta_{i,2}, \alpha_{\theta,2}, \beta_{\theta,2})$ be a vector of continuation

variables, and consider the restricted continuation problem defined by

$$\Phi : u \mapsto \begin{pmatrix} A_{i,1} - \alpha_{i,1} \\ A_{\omega,1} - \alpha_{\omega,1} \\ A_{\theta,1} - \alpha_{\theta,1} \\ B_{i,1} - \beta_{i,1} \\ B_{\omega,1} - \beta_{\omega,1} \\ B_{\theta,1} - \beta_{\theta,1} \\ A_{i,2} - \alpha_{i,2} \\ A_{\omega,2} - \alpha_{\omega,2} \\ A_{\theta,2} - \alpha_{\theta,2} \\ B_{i,2} - \beta_{i,2} \\ B_{\omega,2} - \beta_{\omega,2} \\ B_{\theta,2} - \beta_{\theta,2} \\ \eta_1 - \eta_2 - 0.01 \\ R_1 - R_2 \\ K_{t1} - K_{t2} \end{pmatrix}, \quad (4.15)$$

$$\Psi : u \mapsto \begin{pmatrix} \eta_1 \\ (\alpha_{\theta,1} + 1)^2 + \beta_{\theta,1}^2 \\ R_1 \\ K_{t,1} \\ (\alpha_{\theta,1} + 1)^2 + \beta_{\theta,2}^2 - (\alpha_{\theta,2} + 1)^2 - \beta_{\theta,2}^2 \end{pmatrix}, \quad (4.16)$$

and $\mathbb{I} = \{3, 4\}$. The dimensional deficit of this problem equals 1. It follows that the family of solutions through any regular solution point is one-dimensional manifold. This manifold is parameterized by η_1 . Each point corresponds to a pair of sets of trigonometric coefficients for two distinct steady-state responses (with subscripts $_1$ and $_2$, respectively) resulting from the inputs $v(t) = \cos \eta_1 t$ and $v(t) = \cos \eta_2 t$, where $\eta_2 = \eta_1 - 0.01$. The corresponding value of the second continuation parameter is the squared distance Δ_1 from the Nyquist curve associated with $\eta = \eta_1$ to -1 , and the fifth continuation parameter evaluates to the difference $\Delta_1 - \Delta_2$ between this squared distance and that for $\eta = \eta_2$.

COCO-compatible encodings of the zero functions and the monitor function are shown in the MATLAB functions `openloopssystemp`, `etadif`, `distnyq`, and `othnyq` below.

```

function [data y] = openloopssystem(prob, data, u)

k1      = data.ok1;
k2      = data.ok2;
k3      = data.ok3;
omega0  = data.ox0(1);
current0 = data.ox0(2);
theta0  = data.ox0(3);
b       = data.b;
J       = data.J;
L       = data.L;
Ke      = data.Ke;
eta     = u(1);
R       = u(2);
Kt      = u(3);
v2r     = u(4);
v2i     = u(5);
v3r     = u(6);
v3i     = u(7);
v4r     = u(8);
v4i     = u(9);
T       = 2*pi/eta;
tstart  = 0;
tsam    = 20*T;
tstep   = T/4;
simout  = sim('simopenloopssystem', 'SrcWorkspace', ...
             'current');
omega   = simout.get('omega');
current = simout.get('current');
theta   = simout.get('theta');
data.x0 = [omega(end); current(end); theta(end)];
tsize   = numel(theta);
fomega  = fft(omega(tsize-4:tsize-1)); %4pts
y       = [v2r-real(fomega(2))/2; v2i-imag(fomega(2))/2];
fcurrent = fft(current(tsize-4:tsize-1)); %4pts
y       = [y; v3r-real(fcurrent(2))/2; ...
          v3i-imag(fcurrent(2))/2];
ftheta  = fft(theta(tsize-4:tsize-1)); %4pts
y       = [y; v4r-real(ftheta(2))/2; ...
          v4i-imag(ftheta(2))/2];

end

```

```

function [data y] = etadif(prob, data, u)
eta1 = u(1);
eta2 = u(2);
y     = eta1-eta2-0.01;
end

```

```

function [data y] = distnyq(prob, data, u)
v4r1 = u(1);
v4i1 = u(2);
y     = (v4r1+1)^2+(v4i1)^2;
end

```

```

function [data y] = othnyq(prob, data, u)
v4r1 = u(1);
v4i1 = u(2);
v4r2 = u(3);
v4i2 = u(4);
y     = (v4r1+1)^2+(v4i1)^2-(v4r2+1)^2-(v4i2)^2;
end

```

To initialize the continuation problem, let u_0 correspond to the steady-state response obtained from harmonic excitation at $\eta = 5$ with $R = 1$ and $K_t = 100$ with $\eta_1 = 5$ and $\eta_2 = 4.99$. The following code uses the `coco` entry-point function to perform continuation along the associated one-dimensional solutions manifold.

```

>> data = struct('ok1', 10, 'ok2', 10, 'ok3', 10, 'b', 1, ...
                'J', 0.4, 'L', 10, 'Ke', 1, 'ox0', [0; 0; 0]);
>> u0 = [5; 1; 100; 0.037; -1.9; 0.039; -0.018; ...
        -0.38; -0.0074];
>> prob = coco_prob();
>> prob = coco_set(prob, 'all', 'TOL', 1e-5);
>> prob = coco_set(prob, 'corr', 'ItMX', 50, 'MaxStep', 0.1);
>> prob = coco_set(prob, 'cont', 'PtMX',
                2000, 'h0', 1, 'h_max', 10, 'NPR', 1, 'al_max', 7);
>> prob = coco_add_func(prob, 'phi1', @openloopsystemp, ...
                data, 'zero', 'u0', u0);
>> prob = coco_add_func(prob, 'phi2', @openloopsystemp, ...
                data, 'zero', 'u0', u0+[-0.01; zeros(8,1)]);
>> prob = coco_add_func(prob, 'phi3', @etadif, data, ...

```

```

        'zero', 'uidx', [1;10]);
>> prob = coco_add_func(prob, 'psi1', @distnyq, data, ...
        'active', 'sqdist', 'uidx', [8; 9]);
>> prob = coco_add_func(prob, 'psi2', @othnyq, data, ...
        'active', 'oth', 'uidx', [8; 9; 17; 18]);
>> prob = coco_add_glue(prob, 'glue', [2 3], [11 12]);
>> prob = coco_add_pars(prob, 'pars', [1 2 3], {'eta', 'R', 'Kt'});
>> prob = coco_addevent(prob, 'ot', 'oth', 0);
>> coco(prob, 'nyq_dist_run', [], 1, {'eta' 'oth' 'sqdist'}, ...
        [4.7 5.1]);
>> lab_nyq_dist = coco_bd_labs(bd_nyq_dist_run, 'ot');
>> chart_othco = coco_read_solution('', 'nyq_dist_run', ...
        lab_nyq_dist(end), 'chart');

```

A projection of the solution manifold onto the $(\eta_1, \Delta_1 - \Delta_2)$ coordinate plane is shown below in Fig. 4.8. At the point where $\Delta_1 = \Delta_2$, $\eta_1 \approx 4.8$ and $\Delta_1 \approx 0.36$ (cf. the initialization in Chap. 3 of η_n and δ).

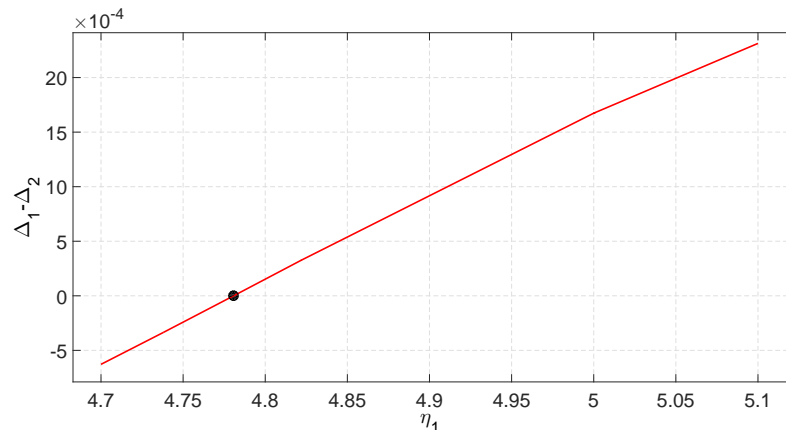


Figure 4.8: Difference in distances to -1 for the frequency response function $H_{V \rightarrow \Omega}(j\eta)/\eta$. Here, the black dot corresponds to the approximate frequency associate with Nyquist distance.

Next, consider the SIMULINK implementation shown in Fig. 4.9 of the feedback structure in Fig. 4.4.

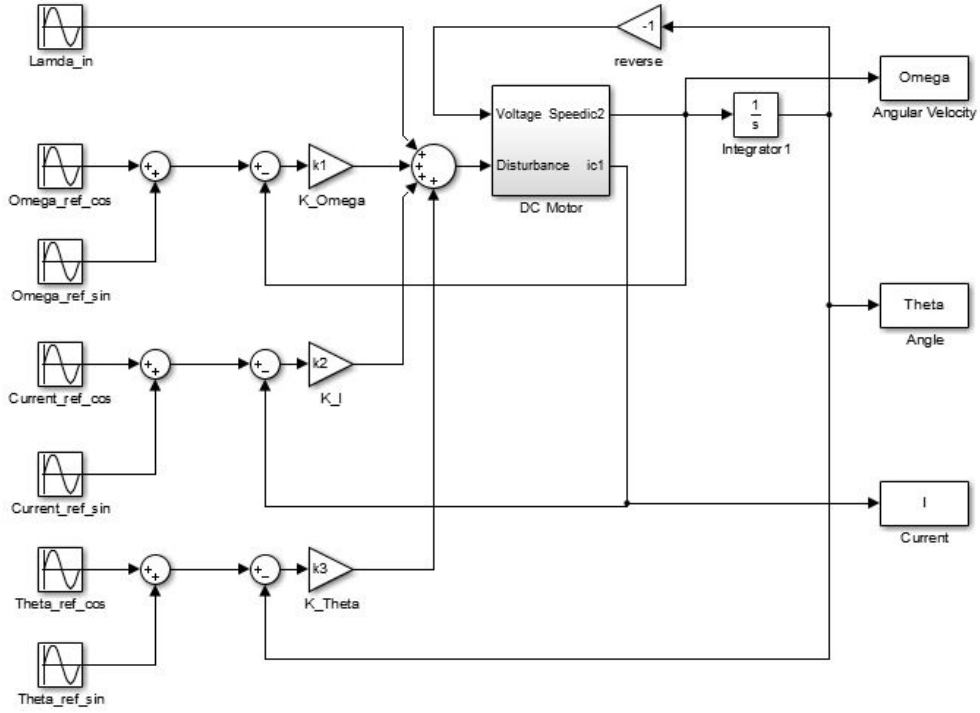


Figure 4.9: SIMULINK model for maximum disturbance detection. The shown system is the disturbance rejection of the superimposed integrator feedback structure 4.4

Let $u = (\eta, R, K_t, \alpha_\omega, \beta_\omega, \alpha_i, \beta_i, \alpha_\theta, \beta_\theta, \nu)$ be a vector of continuation variables, and consider the restricted continuation problem defined by

$$\Phi : u \mapsto \begin{pmatrix} A_i - \alpha_i \\ A_\omega - \alpha_\omega \\ A_\theta - \alpha_\theta \\ B_i - \beta_i \\ B_\omega - \beta_\omega \\ B_\theta - \beta_\theta \\ \alpha_\omega^2 + \beta_\omega^2 - \nu \end{pmatrix}, \quad (4.17)$$

$$\Psi : u \mapsto \begin{pmatrix} \nu \\ \eta \\ R \\ K_t \end{pmatrix}, \quad (4.18)$$

and $\mathbb{I} = \{3, 4\}$. The dimensional deficit of this problem equals 1. It fol-

lows that the family of solutions through any regular solution point is one-dimensional manifold. This manifold is parameterized by η . Each point corresponds to a unique set of trigonometric coefficients for the steady-state responses and phase ϕ of $\theta(t)$ resulting from the input $\lambda(t) = \cos \eta t$. The corresponding value of ν is the squared amplitude of $\omega(t)$.

The MATLAB function `closeloopsystem` below contain COCO-compatible encodings of the zero functions and the monitor function.

```
function [data y] = closeloopsystem(prob, data, u)
k1      = data.ck1;
k2      = data.ck2;
k3      = data.ck3;
omega0  = data.cx0(1);
current0 = data.cx0(2);
theta0  = data.cx0(3);
b       = data.b;
J       = data.J;
L       = data.L;
Ke      = data.Ke;
eta     = u(1);
R       = u(2);
Kt      = u(3);
v2r     = u(4);
v2i     = u(5);
v3r     = u(6);
v3i     = u(7);
v4r     = u(8);
v4i     = u(9);
mag     = u(10);
T       = 2*pi/eta;
tstart  = 0;
tsam    = 20*T;
tstep   = T/4;
simout  = sim('simcloseloopsystem', ...
             'SrcWorkspace', 'current');
omega   = simout.get('omega');
current = simout.get('current');
theta   = simout.get('theta');
data.cx0 = [omega(end); current(end); theta(end)];
tsize   = numel(omega);
fomega  = fft(omega(tsize-4:tsize-1)); %4pts
```

```

y          = [v2r-real(fomega(2))/2; v2i-imag(fomega(2))/2];
fcurrent  = fft(current(tsize-4:tsize-1)); %4pts
y          = [y; v3r-real(fcurrent(2))/2; ...
             v3i-imag(fcurrent(2))/2];
ftheta    = fft(theta(tsize-4:tsize-1)); %4pts
y          = [y; v4r-real(ftheta(2))/2; v4i-imag(ftheta(2))/2];
y          = [y; (abs(fomega(2)/2))^2-mag];
end

```

Here, `simcloseloopssystem` refers to the SIMULINK model of the closed-loop system (see Fig. 4.9). To initialize the continuation problem, let u_0 correspond to the steady-state response obtained from harmonic excitation at $\eta = 3$ with $R = 1$ and $K_t = 100$. The following code uses the `coco` entry-point function to perform continuation along the associated one-dimensional solutions manifold.

```

>> data = struct('k1', 10, 'k2', 10, 'k3', 10, 'b', 1, ...
                'J', 0.4, 'L', 10, 'Ke', 1, 'x0', [0; 0; 0]);
>> u0    = [3; 1; 100; 2.3643e-04; 0.4615; ...
            -0.0155; 0.0046; 0.4615; 0.1333; 0.0402];
>> prob = coco_prob();
>> prob = coco_set(prob, 'cont', 'PtMX', 1000, 'h0', 1, ...
                    'h_max', 50, 'al_max', 10, 'NPR', 1);
>> prob = coco_set(prob, 'corr', 'TOL', 1.0e-5);
>> prob = coco_add_func(prob, 'plinit_c_phi1', ...
                        @closeloopssystem, data, 'zero', 'u0', u0);
>> prob = coco_add_pars(prob, 'plinit_c_psi1', 10, 'mag');
>> prob = coco_add_pars(prob, 'pars', [1 2 3], ...
                        {'eta', 'R', 'Kt'});
>> bd_maxmag = coco(prob, 'maxmagdetect', [], 1, ...
                   {'mag' 'eta'}, [0.1 5]);
>> lab_maxmag = coco_bd_labs(bd_maxmag, 'FP');
>> chart_maxmu = coco_read_solution('', 'maxmagdetect', ...
                                   lab_maxmag, 'chart');

```

A projection of the solution manifold onto the (η, ν) coordinate plane is shown below in Fig. 4.10. The maximum value of ν is detected as a fold point along the solution manifold at $\eta \approx 4.9$, the maximum value of ν is approximated 2.5108 (cf. the initialization in Chap. 3 of η_m).

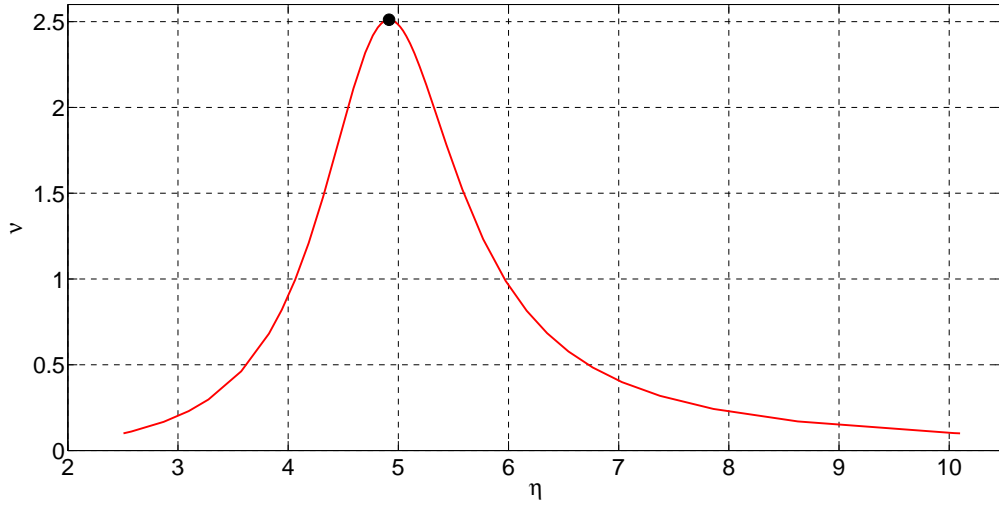


Figure 4.10: Magnitude for the frequency response function $(j\eta)H_{\Lambda \rightarrow \Omega}(j\eta)/((j\eta) + H_{V \rightarrow \Omega}(j\eta))$. Here, the black dot corresponds to the frequency of the minimum disturbance rejection.

4.3 Constant Gain Margin

For the constant gain margin optimization problem, let

$$u = \begin{pmatrix} \eta_1, R_1, K_{t,1}, \alpha_{\omega,1}, \beta_{\omega,1}, \alpha_{i,1}, \beta_{i,1}, \alpha_{\theta,1}, \beta_{\theta,1}, \phi, \\ \eta_2, R_2, K_{t,2}, \alpha_{\omega,2}, \beta_{\omega,2}, \alpha_{i,2}, \beta_{i,2}, \alpha_{\theta,2}, \beta_{\theta,2}, \nu_2, \\ \eta_3, R_3, K_{t,3}, \alpha_{\omega,3}, \beta_{\omega,3}, \alpha_{i,3}, \beta_{i,3}, \alpha_{\theta,3}, \beta_{\theta,3}, \nu_3 \end{pmatrix} \quad (4.19)$$

be a vector of continuation variables, and consider the restricted continuation problem defined by

$$\Phi : u \mapsto \begin{pmatrix} A_{i,1} - \alpha_{i,1} \\ A_{\omega,1} - \alpha_{\omega,1} \\ A_{\theta,1} - \alpha_{\theta,1} \\ B_{i,1} - \beta_{i,1} \\ B_{\omega,1} - \beta_{\omega,1} \\ B_{\theta,1} - \beta_{\theta,1} \\ \beta_{\theta,1} \cos \phi - \alpha_{\theta,1} \sin \phi \\ A_{i,2} - \alpha_{i,2} \\ A_{\omega,2} - \alpha_{\omega,2} \\ A_{\theta,2} - \alpha_{\theta,2} \\ B_{i,2} - \beta_{i,2} \\ B_{\omega,2} - \beta_{\omega,2} \\ B_{\theta,2} - \beta_{\theta,2} \\ \alpha_{\omega,2}^2 + \beta_{\omega,2}^2 - \nu_2 \\ A_{i,3} - \alpha_{i,3} \\ A_{\omega,3} - \alpha_{\omega,3} \\ A_{\theta,3} - \alpha_{\theta,3} \\ B_{i,3} - \beta_{i,3} \\ B_{\omega,3} - \beta_{\omega,3} \\ B_{\theta,3} - \beta_{\theta,3} \\ \alpha_{\omega,3}^2 + \beta_{\omega,3}^2 - \nu_3 \\ \eta_2 - \eta_3 - 0.01 \\ \nu_2 - \nu_3 \\ R_1 - R_2 \\ K_{t,1} - K_{t,2} \\ R_2 - R_3 \\ K_{t,2} - K_{t,3} \end{pmatrix}, \quad (4.20)$$

$$\Psi : u \mapsto \begin{pmatrix} \alpha_{\theta,1}^2 + \beta_{\theta,1}^2 \\ R_1 \\ K_{t,1} \\ \phi \\ \nu_2 \end{pmatrix}, \quad (4.21)$$

and $\mathbb{I} = \{1, 4\}$. The dimensional deficit of this problem equals 1. It follows that the family of solutions through any regular solution point is one-

dimensional manifold. Each point on this manifold corresponds to three coupled experiments in which constraints are imposed on the steady-state response. Specifically, subscript $_1$ denotes an instance of the first elementary experiment, whereas subscripts $_2$ and $_3$ denote instances of the second elementary experiment, for excitation frequencies that differ by 0.01, but with identical amplitudes of $\omega(t)$. The choice of inactive continuation parameters ensures that the gain margin is constant provided that the value of the fourth continuation parameter equals $-\pi$.

The functions `openloopssystem`, `closeloopssystem`, and `ampitude` have been introduced in the previous section. `coco`-compatible encodings of the MATLAB functions `closeloopdiff` and `closelopeqdist` are shown below.

```
function [data y] = closeloopdiff(prob, data, u)
eta1 = u(1);
eta2 = u(2);
y     = eta1-eta2-0.01;
end
```

```
function [data y] = closelopeqdist(prob, data, u)
mag1 = u(1);
mag2 = u(2);
y     = mag1-mag2;
end
```

To initialize the continuation problem, let `uopen` correspond to the phase crossover frequency and the corresponding steady-state response obtained from the frequency sweep in Fig. 4.6. Let `uclose` correspond to the frequency associated with the maximum steady-state response magnitude of $\omega(t)$ for a harmonic torque disturbance and the corresponding steady-state response obtained from the frequency sweep in Fig. 4.10. The following code uses the `COCO` entry-point function to perform continuation along the associated one-dimensional solutions manifold.

```
>> data = struct('ok1', 10, 'ok2', 10, 'ok3', 10, ...
                'ck1', 10, 'ck2', 5, 'ck3', 10, 'b', 1, ...
                'J', 0.4, 'L', 10, 'Ke', 1, ...
```

```

        'ox0', [0; 0; 0 ], 'cx0', [0; 0; 0 ]);
>> u_open = chart_phsco.x(1:10);
>> u_close = [chart_maxmu.x(1:10)];
>> prob = coco_prob();
>> prob = coco_set(prob, 'all', 'TOL', 1e-5);
>> prob = coco_set(prob, 'corr', 'ItMX', 50);
>> prob = coco_set(prob, 'cont', 'PtMX', 2000, ...
        'h0', 1, 'h_max', 100, 'h_fac_min', ...
        0.1, 'NPR', 1);
>> prob = coco_add_func(prob, 'pl_coco_phi1', ...
        @openloopssystem, data, 'zero', 'u0', u_open);
>> prob = coco_add_func(prob, 'pl_coco_phi2', ...
        @closeloopssystem, data, 'zero', 'u0', u_close);
>> prob = coco_add_func(prob, 'pl_coco_phi3', ...
        @closeloopssystem, data, 'zero', ...
        'u0', u_close+[-0.01;zeros(9,1)]);
>> prob = coco_add_func(prob, 'pl_coco_phi4', ...
        @closeloop_diff, data, 'zero', 'uidx', [11;21]);
>> prob = coco_add_func(prob, 'pl_coco_phi5', ...
        @closeloop_eqdist, data, 'zero', 'uidx', [20 30]);
>> prob = coco_add_glue(prob, 'pl_coco_glue1', ...
        [2 3], [12 13]);
>> prob = coco_add_glue(prob, 'pl_coco_glue2', ...
        [12 13], [22 23]);
>> prob = coco_add_func(prob, 'pl_coco_psi1', ...
        @amplitude, data, 'inactive', 'sqmag', ...
        'uidx', [8 9]);
>> prob = coco_add_pars(prob, 'pars', [2 3 10 20], ...
        {'R', 'Kt', 'phase', 'mu'});
>> prob = coco_set_parival(prob, 'sqmag', 0.3808^2);
>> prob = coco_set_parival(prob, 'phase', -pi);
>> coco(prob, 'PlMuRkt_COCO_S', [], 1, {'mu' 'Kt' 'R'}, ...
        {[0 5], [1 300], [0.1 300]});

```

A projection of the solution manifold onto the $(\nu_2, R_1, K_{t,1})$ coordinate space is shown in Fig. 4.11. This figure also includes the corresponding results from Chap. 3 for comparison. Note that although the frequencies η_2 and η_3 deviate slightly from η_m , the agreement is very good.

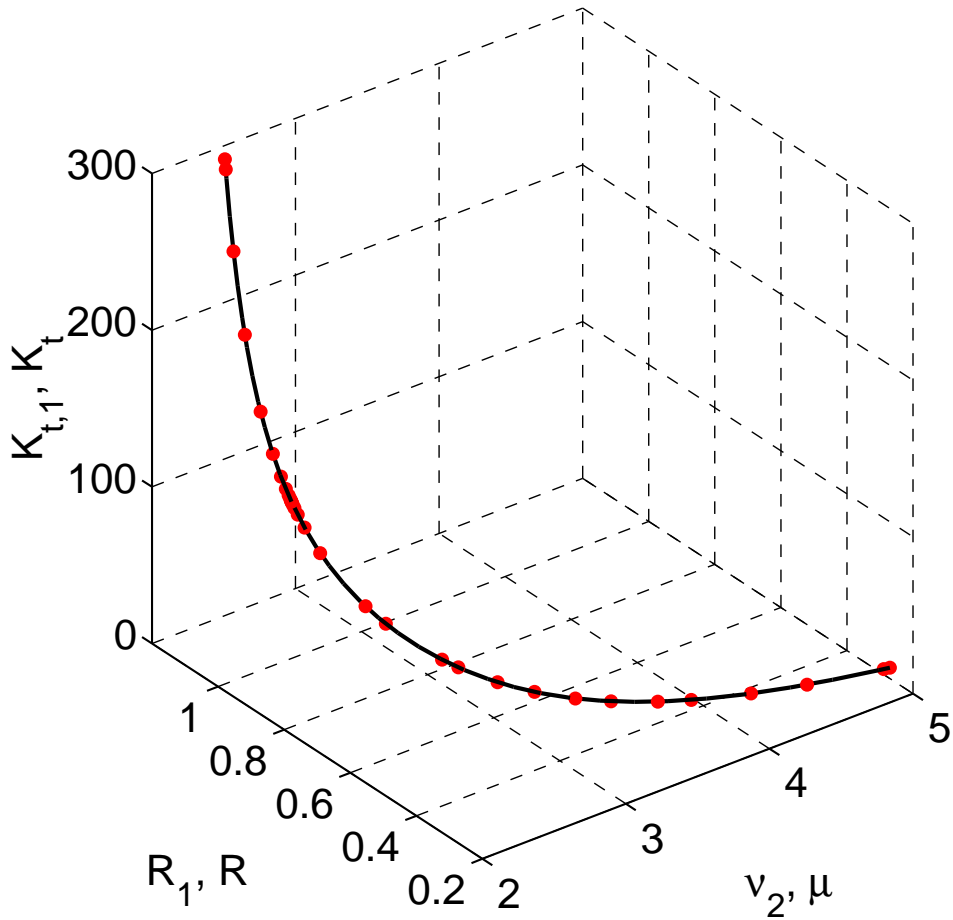


Figure 4.11: The results (red dots) from control-based continuation agree with those (solid) obtained using algebraic continuation for the constant gain margin optimization problem.

4.4 Constant Phase Margin

Consider the identical continuation problem as in the previous section, but let u_{open} correspond to the gain crossover frequency and the corresponding steady-state response obtained from the frequency sweep in Fig. 4.7. The following code uses the `coco` entry-point function to perform continuation along the associated one-dimensional solutions manifold.

```
>> data = struct('ok1', 10, 'ok2', 10, 'ok3', 10, ...
```

```

        'ck1', 10, 'ck2', 5, 'ck3', 10, 'b', 1, ...
        'J', 0.4, 'L', 10, 'Ke', 1, 'ox0', [0; 0; 0 ], ...
        'cx0', [0; 0; 0 ]);
>> u_open = chart_magco.x(1:10);
>> u_close = [chart_maxmu.x(1:10)];
>> prob = coco_prob();
>> prob = coco_set(prob, 'all', 'TOL', 1e-5);
>> prob = coco_set(prob, 'corr', 'ItMX', 50);
>> prob = coco_set(prob, 'cont', 'PtMX', 2000, 'h0', 1, ...
        'h_max', 100, 'NPR', 1, 'h_fac_min', 0.1);
>> prob = coco_add_func(prob, 'phi1', @openloopssystem, ...
        data, 'zero', 'u0', u_open);
>> prob = coco_add_func(prob, 'phi2', @closeloopssystem, ...
        data, 'zero', 'u0', u_close);
>> prob = coco_add_func(prob, 'phi3', @closeloopssystem, ...
        data, 'zero', 'u0', u_close+[-0.01;zeros(9,1)]);
>> prob = coco_add_func(prob, 'phi4', @closeloopdiff, ...
        data, 'zero', 'uidx', [11;21]);
>> prob = coco_add_func(prob, 'phi5', @closeloopseqdist, ...
        data, 'zero', 'uidx', [20;30]);
>> prob = coco_add_glue(prob, 'glue1', [2 3], [12 13]);
>> prob = coco_add_glue(prob, 'glue2', [2 3], [22 23]);
>> prob = coco_add_func(prob, 'psil', @amplitude, data, ...
        'inactive', 'sqmag', 'uidx', [8 9]);
>> prob = coco_add_pars(prob, 'pars', [2 3 10 20], ...
        {'R', 'Kt', 'phase', 'mu'});
>> prob = coco_set_parival(prob, 'sqmag', 1);
>> prob = coco_set_parival(prob, 'phase', -1.6807);
>> coco(prob, 'P2MuRKt_COCO', [], 1, {'mu' 'Kt' 'R'}, ...
        {[0 5], [1 300], [0.1 300]});

```

A projection of the solution manifold onto the $(\nu_2, R_1, K_{t,1})$ coordinate space is shown below in Fig. 4.12. This figure also includes the corresponding results from Chap. 3 for comparison. Note that although the frequencies η_2 and η_3 deviate slightly from η_m , the agreement is very good.

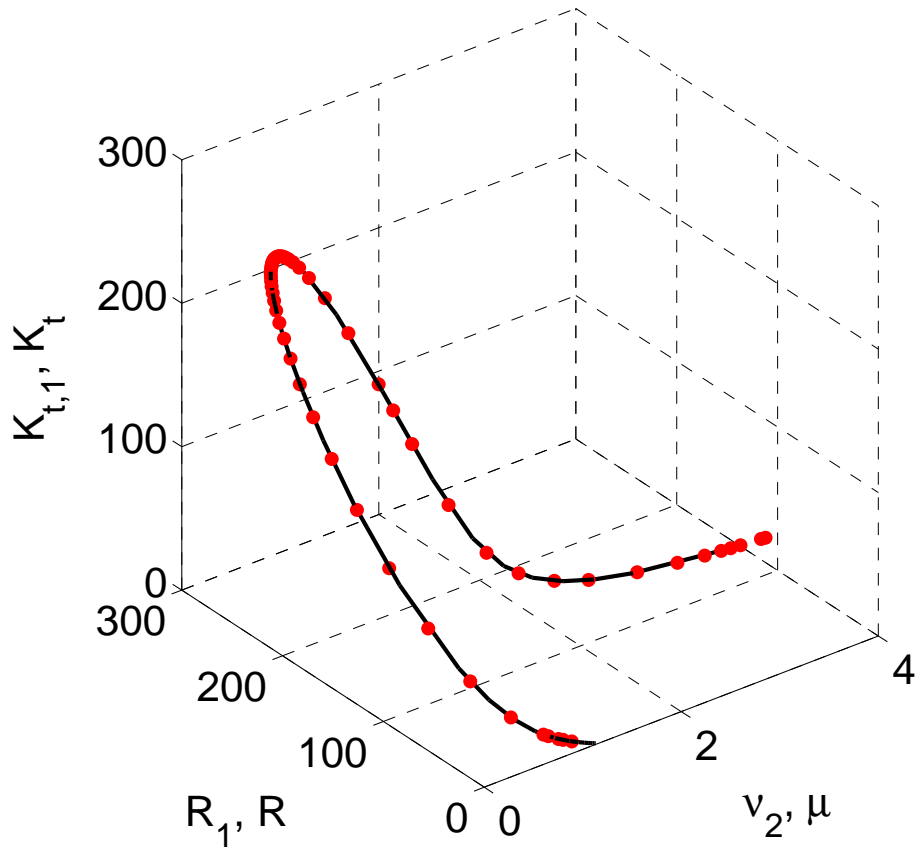


Figure 4.12: The results (red dots) from control-based continuation agree with those (solid) obtained using algebraic continuation for the constant phase margin optimization problem.

4.5 Constant Nyquist Distance

Next, let

$$u = \begin{pmatrix} \eta_1, R_1, K_{t1}, \alpha_{\omega,1}, \beta_{\omega,1}, \alpha_{i,1}, \beta_{i,1}, \alpha_{\theta,1}, \beta_{\theta,1}, \\ \eta_2, R_2, K_{t2}, \alpha_{\omega,2}, \beta_{\omega,2}, \alpha_{i,2}, \beta_{i,2}, \alpha_{\theta,2}, \beta_{\theta,2}, \\ \eta_3, R_3, K_{t3}, \alpha_{\omega,3}, \beta_{\omega,3}, \alpha_{i,3}, \beta_{i,3}, \alpha_{\theta,3}, \beta_{\theta,3}, \nu_3, \\ \eta_4, R_4, K_{t4}, \alpha_{\omega,4}, \beta_{\omega,4}, \alpha_{i,4}, \beta_{i,4}, \alpha_{\theta,4}, \beta_{\theta,4}, \nu_4 \end{pmatrix} \quad (4.22)$$

be a vector of continuation variables, and consider restricted continuation problem defined by

$$\Phi : u \mapsto \begin{pmatrix} F_1 \\ F_2 \\ F_3 \end{pmatrix}, \quad (4.23)$$

where

$$F_1 = \begin{pmatrix} A_{i,1} - \alpha_{i,1} \\ A_{\omega,1} - \alpha_{\omega,1} \\ A_{\theta,1} - \alpha_{\theta,1} \\ B_{i,1} - \beta_{i,1} \\ B_{\omega,1} - \beta_{\omega,1} \\ B_{\theta,1} - \beta_{\theta,1} \\ A_{i,2} - \alpha_{i,2} \\ A_{\omega,2} - \alpha_{\omega,2} \\ A_{\theta,2} - \alpha_{\theta,2} \\ B_{i,2} - \beta_{i,2} \\ B_{\omega,2} - \beta_{\omega,2} \\ B_{\theta,2} - \beta_{\theta,2} \end{pmatrix}, \quad (4.24)$$

$$F_2 = \begin{pmatrix} A_{i,3} - \alpha_{i,3} \\ A_{\omega,3} - \alpha_{\omega,3} \\ A_{\theta,3} - \alpha_{\theta,3} \\ B_{i,3} - \beta_{i,3} \\ B_{\omega,3} - \beta_{\omega,3} \\ B_{\theta,3} - \beta_{\theta,3} \\ \alpha_{\omega,3}^2 + \beta_{\omega,3}^2 - \nu_3 \\ A_{i,4} - \alpha_{i,4} \\ A_{\omega,4} - \alpha_{\omega,4} \\ A_{\theta,4} - \alpha_{\theta,4} \\ B_{i,4} - \beta_{i,4} \\ B_{\omega,4} - \beta_{\omega,4} \\ B_{\theta,4} - \beta_{\theta,4} \\ \alpha_{\omega,4}^2 + \beta_{\omega,4}^2 - \mu_4 \end{pmatrix}, \quad (4.25)$$

$$F_3 = \begin{pmatrix} \eta_1 - \eta_2 - 0.01 \\ \eta_3 - \eta_4 - 0.01 \\ \nu_3 - \nu_4 \\ R_1 - R_2 \\ K_{t1} - K_{t2} \\ R_1 - R_3 \\ K_{t1} - K_{t3} \\ R_1 - R_4 \\ K_{t1} - K_{t4} \end{pmatrix}, \quad (4.26)$$

$$\Psi : u \mapsto \begin{pmatrix} R \\ K_t \\ (\alpha_{\theta,1} + 1)^2 + \beta_{\theta,2}^2 - (\alpha_{\theta,2} + 1)^2 - \beta_{\theta,2}^2 \\ (\alpha_{\theta,1} + 1)^2 + \beta_{\theta,2}^2 \\ \nu_3 \end{pmatrix}, \quad (4.27)$$

and $\mathbb{I} = \{3, 4\}$. The dimensional deficit of this problem equals 1. It follows that the family of solutions through any regular solution point is one-dimensional manifold. Each point on this manifold corresponds to four coupled experiments in which constraints are imposed on the steady-state response. Specifically, subscripts $_1$ and $_2$ denote instances of the first elementary experiment, whereas subscripts $_3$ and $_4$ denote instances of the second elementary experiment. For the two instances of each experiment, the frequencies of excitation differ by 0.01. The choice of inactive continuation parameters ensures that the approximated Nyquist distance is constant provided that the value of the third continuation parameter equals zero.

The function `openloopssystem`, `closeloopssystem`, `closeloopdiff`, `closeloopreqdist`, `distnyq`, `othnyq`, `etadiff` and `coco.add_glue` have been introduced in the previous section. To initialize the continuation problem, let `u_open` correspond to the minimum Nyquist distance frequency and the corresponding steady-state response obtained from the frequency sweep in Fig. 4.8. Let `u_close` correspond to the frequency associated with the maximum steady-state response magnitude of $\omega(t)$ for a harmonic torque disturbance and the corresponding steady-state response obtained from the frequency sweep in Fig. 4.10. The following code uses the `coco` entry-point function to perform continuation along the associated one-dimensional solutions manifold.


```

>> data = struct('ok1', 10, 'ok2', 10, 'ok3', 10, ...
    'ck1', 10, 'ck2', 5, 'ck3', 10, 'b', 1, ...
    'J', 0.4, 'L', 10, 'Ke', 1, 'ox0', [0; 0; 0 ], ...
    'cx0', [0; 0; 0 ]);
>> u_open = chart_othco.x(1:9);
>> u_close = chartmaxmu.x(1:10);
>> prob = coco_prob();
>> prob = coco_set(prob, 'all', 'TOL', 1e-5);
>> prob = coco_set(prob, 'corr', 'ItMX', 50, 'MaxStep', 0.1);
>> prob = coco_set(prob, 'cont', 'PtMX', 2000, 'h0', 1, ...
    'h_max', 15, 'NPR', 1, 'FP', true);
>> prob = coco_add_func(prob, 'phi1', @openloopssystem, ...
    data, 'zero', 'u0', u_open);
>> prob = coco_add_func(prob, 'phi2', @openloopssystem, ...
    data, 'zero', 'u0', u_open+[-0.01, zeros(8,1)]);
>> prob = coco_add_func(prob, 'phi3', @closeloopssystem, ...
    data, 'zero', 'u0', u_close);
>> prob = coco_add_func(prob, 'phi4', @closeloopssystem, ...
    data, 'zero', 'u0', u_close+[-0.01; zeros(9,1)]);
>> prob = coco_add_func(prob, 'phi5', @closeloopdiff, ...
    data, 'zero', 'uidx', [19;29]);
>> prob = coco_add_func(prob, 'phi6', @etadif, data, ...
    'zero', 'uidx', [1;10]);
>> prob = coco_add_func(prob, 'phi7', @closeloopseqdist, ...
    data, 'zero', 'uidx', [28;38]);
>> prob = coco_add_glue(prob, 'glue1', [2 3], [11 12]);
>> prob = coco_add_glue(prob, 'glue2', [2 3], [20 21]);
>> prob = coco_add_glue(prob, 'glue3', [2 3], [30 31]);
>> prob = coco_add_func(prob, 'psil', @dist_nyq, data, ...
    'inactive', 'sqdist', 'uidx', [8; 9]);
>> prob = coco_add_func(prob, 'psi2', @oth_nyq, data, ...
    'inactive', 'oth', 'uidx', [8; 9; 17; 18]);
>> prob = coco_add_pars(prob, 'pars', [2 3 28], ...
    {'R', 'Kt', 'mu'});
>> prob = coco_set_parival(prob, 'sqdist', 0.36);
>> prob = coco_set_parival(prob, 'oth', 0);
>> coco(prob, 'P3MuRkt_COCO', [], 1, {'mu' 'Kt' 'R'}, ...
    {[0 5], [1 300], [0.1 300]});

```

A projection of the solution manifold onto the $(\nu_3, R_1, K_{t,1})$ coordinate space is shown below in Fig. 4.13. This figure also includes the corresponding results from Chap. 3 for comparison. Note that although the frequencies η_1 and η_2 deviate slightly from η_m , and η_3 and η_4 deviate slightly from η_m , the

agreement is very good.

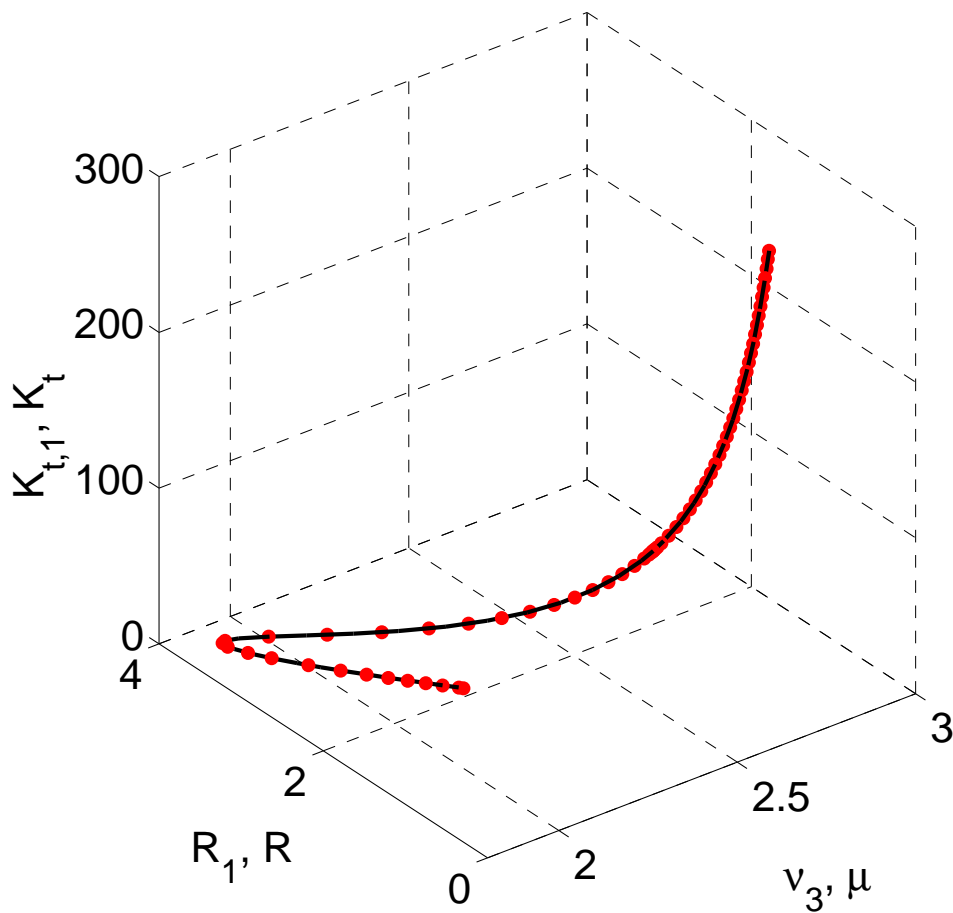


Figure 4.13: The results (red dots) from control-based continuation agree with those (solid) obtained using algebraic continuation for the constant Nyquist distance optimization problem.

4.6 Discussion

In this chapter, we have formulated the continuation problems for simulated experiments and analyzed the same optimal design problems as in Chap. 3 based on measurable outputs only. The results verify that it is possible to find the parametric manifold associated with solutions of a system of equations without having explicit expressions for these equations. This is especially useful for actual experiments with unmodeled dynamics. In the following

chapter, we will describe an alternative implementation that substitutes an iterated method for approximating the problem Jacobian instead of finite differences.

CHAPTER 5

THE CONTINEX TOOLBOX

The implementation of COCO used in the previous chapters relies on an iterated Newton solver for locating points on the solution manifold. In the absence of explicit derivatives for the continuation variables, it is necessary to approximate the Jacobian that appears in Newton's method. In the previous chapters, the default algorithm uses a first-order finite-difference scheme to estimate the Jacobian. Such an implementation requires repeated evaluation of the zero and monitor functions, which can be time-consuming if simulations are run every iteration. The number of such evaluations per Newton step equals the number of continuation variables plus 1.

This chapter describes the use of the Broyden method, implemented in the COCO-compatible CONTINEX toolbox [28], for updating an approximation of parts of the problem Jacobian in each Newton step. The Broyden update uses a previous approximation obtained either by finite differences or by a previous iteration of Broyden's method. If no previous approximation exists, then by default CONTINEX initializes the matrix to an identity matrix padded with zero columns. This initialization causes a singular problem matrix in cases where additional constraints are imposed on coupled instances of the CONTINEX toolbox. In the analysis described below, this was addressed by initializing the matrix to an identity matrix padded with columns with small amplitude random entries.

5.1 Numerical Results

The CONTINEX implementation of the continuation problems formulated in Chap. 4 is similar to the implementation shown there with only a few changes to fit the syntax of CONTINEX. The codes for implementing each of the elementary experiments are shown in Appendix A. The implementation of the

three coupled design problems can be found in Appendix B. The corresponding results are shown in Figs. 5.1-5.3 and agree closely with the predictions from Chap. 4.

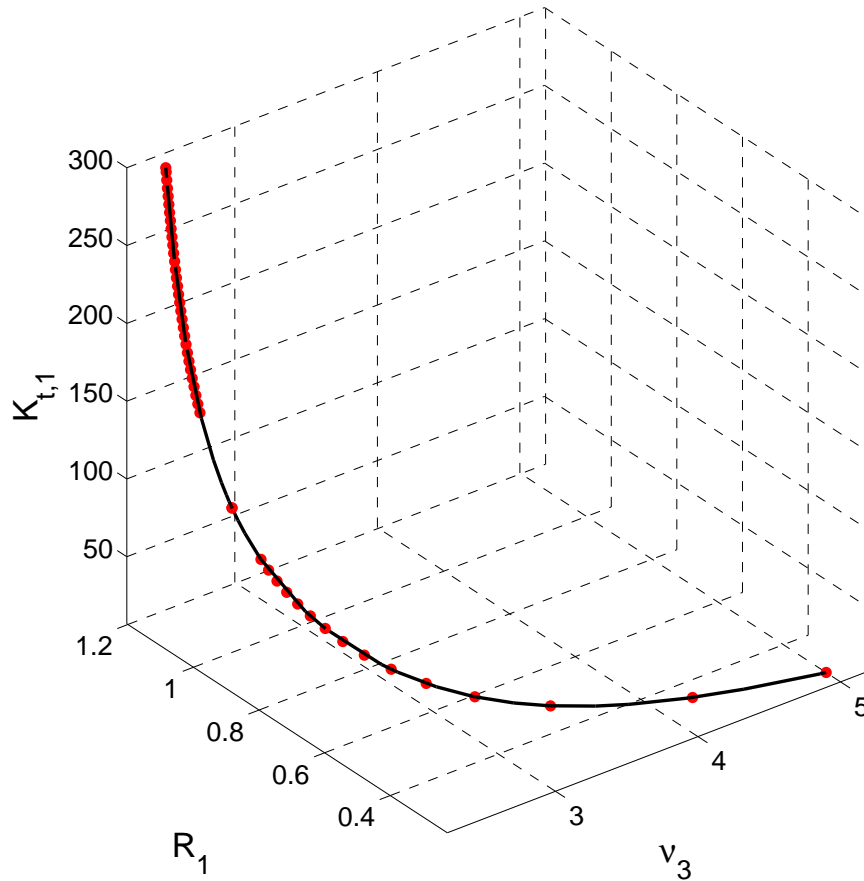


Figure 5.1: The results (red dots) from continuation using CONTINEX agree with those obtained in Chap. 4 using control-based continuation (black solid) for the constant gain margin problem.

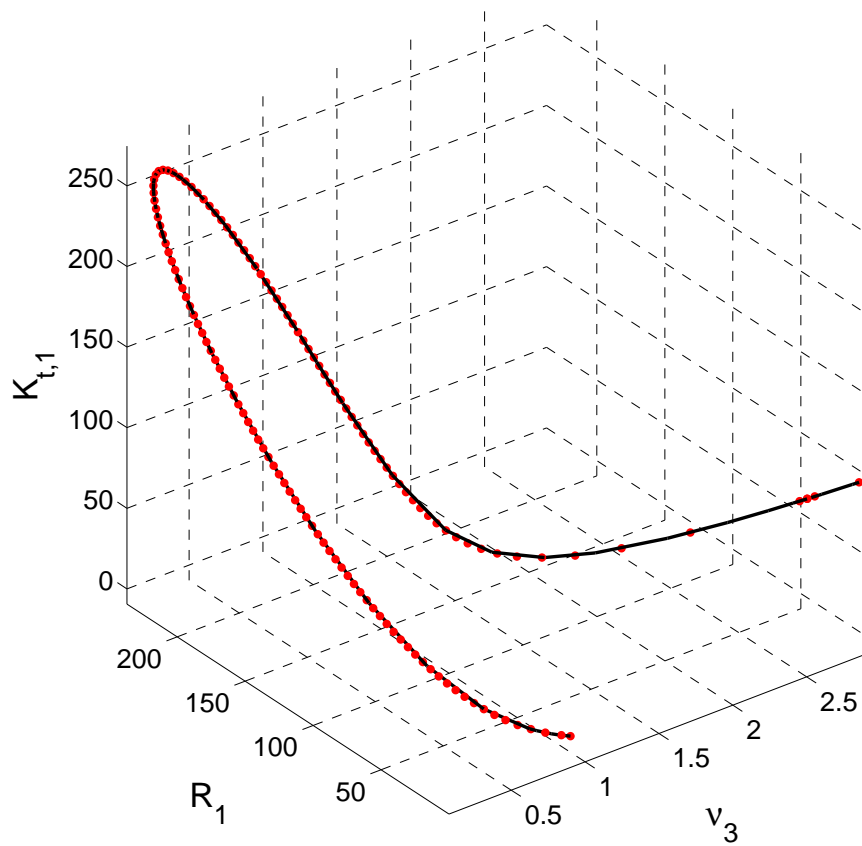


Figure 5.2: The results (red dots) from continuation using CONTINEX agree with those obtained in Chap. 4 using control-based continuation (black solid) for the constant phase margin problem.

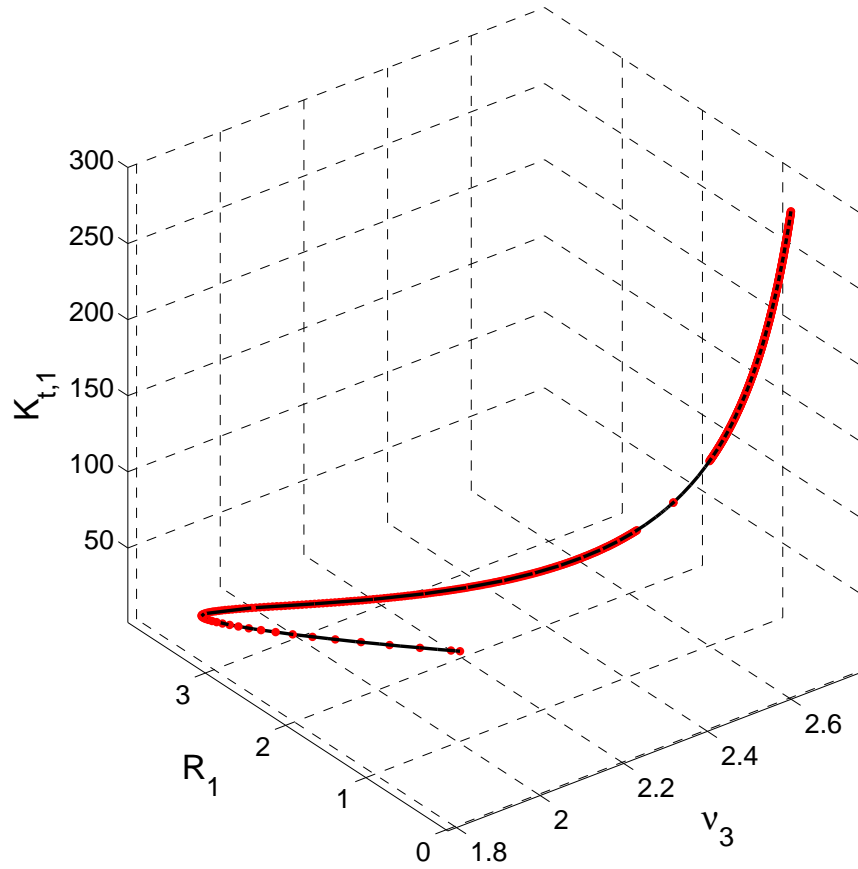


Figure 5.3: The results (red dots) from continuation using CONTINEX agree with those obtained in Chap. 4 using control-based continuation (black solid) for the constant Nyquist distance problem.

To compare the computational efficiency of the CONTINEX implementation and the method used in Chap. 4, it is instructive to inspect the initial part of the screen output from the COCO run. In Chap. 4, each point on the solution manifold is located using Newton iterates with approximate Jacobians obtained using finite differences. The initial part of the screen output in Fig. 5.4 shows the convergence to a starting point on the solution manifold from the initial solution guess. Here, convergence is achieved after five iterates and 50 seconds of computation time.

STEP	DAMPING		NORMS			COMPUTATION TIMES		
IT	SIT	GAMMA	d	f	U	F(x)	DF(x)	SOLVE
0				6.35e-01	2.00e+02	0.3	0.0	0.0
1	1	7.67e-01	6.58e-01	1.48e-01	2.00e+02	0.6	7.0	0.0
2	1	1.00e+00	3.96e-01	9.43e-02	2.00e+02	0.9	14.1	0.0
3	1	1.00e+00	8.65e-02	1.84e-03	2.00e+02	1.3	21.3	0.0
4	1	1.00e+00	2.41e-03	1.16e-06	2.00e+02	1.6	28.3	0.0
5	1	1.00e+00	2.44e-06	1.71e-12	2.00e+02	1.9	35.2	0.0

STEP	TIME	U	LABEL	TYPE	mu	Kt	R
0	00:00:50	2.0029e+02	1	EP	2.5121e+00	1.0000e+02	1.0004e+00

Figure 5.4: Screen printout of the initial convergence to a starting point on the solution manifold for the constant gain margin problem using finite-difference approximations of the problem Jacobian.

In CONTINEX, each point on the solution manifold is located using Newton iterates with approximate Jacobians obtained using simultaneous Broyden updates. The initial part of the screen output in Fig. 5.5 shows the convergence to a starting point on the solution manifold from the initial solution guess. Here, convergence is achieved after 21 iterates and 25 seconds of computation time.

STEP		DAMPING		NORMS			COMPUTATION TIMES		
IT	SIT	#	GAMMA	d	f	U	F(x)	DF(x)	SOLVE
0					6.35e-01	2.00e+02	0.0	0.0	0.0
1	1		6.58e-01	2.00e+01	2.22e-01	1.87e+02	0.4	3.9	0.0
2	1		1.69e-01	1.74e+02	1.90e-01	2.17e+02	0.8	4.0	0.0
3	1		9.08e-01	3.79e+01	3.98e-02	1.82e+02	1.2	4.1	0.0
4	4		1.25e-01	4.48e+00	4.41e-02	1.82e+02	2.7	4.2	0.0
5	4		1.25e-01	1.47e+00	4.39e-02	1.81e+02	4.4	4.3	0.0
6	4		1.25e-01	5.16e-01	4.40e-02	1.81e+02	5.9	4.4	0.0
7	4		1.25e-01	2.13e-01	4.41e-02	1.81e+02	7.5	4.5	0.0
8	4		1.25e-01	3.04e-01	4.40e-02	1.81e+02	9.0	4.6	0.0
9	1		1.00e+00	6.54e-01	3.75e-02	1.82e+02	9.5	4.7	0.0
10	1		1.00e+00	4.07e-01	2.00e-03	1.82e+02	9.8	4.8	0.0
11	1		1.00e+00	3.48e+00	9.39e-04	1.86e+02	10.2	8.6	0.0
12	2		5.00e-01	1.26e+01	3.31e-04	1.92e+02	10.9	8.7	0.0
13	2		5.00e-01	8.19e+00	2.99e-04	1.96e+02	11.8	8.8	0.0
14	1		1.00e+00	3.79e+00	1.42e-04	2.00e+02	12.1	8.9	0.0
15	1		1.00e+00	6.42e-02	4.44e-06	2.00e+02	12.5	9.0	0.0
16	2		5.00e-01	2.09e-01	4.32e-06	2.00e+02	13.3	9.1	0.0
17	1		1.00e+00	5.51e-02	2.30e-08	2.00e+02	13.7	9.2	0.0
18	1		1.00e+00	2.79e-04	1.30e-09	2.00e+02	14.1	9.3	0.0
19	1	1	1.00e+00	3.94e-06	3.91e-11	2.00e+02	14.4	9.4	0.0
20	1	2	1.00e+00	8.45e-08	2.08e-11	2.00e+02	14.8	9.5	0.0
21	1	3	1.00e+00	4.73e-09	1.37e-11	2.00e+02	15.2	9.6	0.0

STEP	TIME	U	LABEL	TYPE	mu	Kt	R
0	00:00:25	1.9994e+02	1	EP	2.5123e+00	9.9826e+01	1.0000e+00

Figure 5.5: Screen printout of the initial convergence to a starting point on the solution manifold for the constant gain margin problem using Broyden updates for the problem Jacobian.

This suggests that Broyden’s method takes less computational time than the implementation based on finite differences. It is also worth noting that Broyden’s method uses more iterations to converge to the solution, which is consistent with the fact that Broyden’s method does not preserve the quadratic convergence of Newton’s method.

CHAPTER 6

CONCLUSIONS

This thesis focuses on the feasibility of applying control-based continuation to solve constrained design problems for periodically excited linear systems. As implemented here, control-based continuation enables the imposition of nontrivial nonlinear constraints on the frequency response of a linear system with opportunities to regulate rates of convergence by the tuning of feedback gains, without access to an explicit model of the system. As an example, the analysis shows the possibility of reducing the angular velocity response of an armature-controlled DC motor to a disturbance torque while imposing constraints on the properties of a suitably defined open-loop transfer function.

The formulation in Chap. 4 of elementary experiments points to the potential implementation of the control-based continuation paradigm in a real-time physical system. Indeed, each SIMULINK model can be replaced by a physical experiment, with complete transparency as far as the COCO implementation is concerned. The CONTINEX toolbox discussed briefly in Chap. 5 is specifically designed to handle noise-contaminated data from such a physical experiment [27]. Future research with the proposed design methodology should consider a coupling of CONTINEX with an appropriate experimental realization of the DC motor and its feedback embeddings.

Although the DC motor model is a linear system, the stability margins and design functions considered in this thesis are nonlinear functions of the system parameters. Linearity is thus not an essential part of this design paradigm. Indeed, the method of control-based continuation can also be used to analyze design problems in which constraints are imposed on the properties of a periodic trajectory of a nonlinear system, whether stable or unstable. In such cases, analytic expressions are rarely available, and a mathematical model may offer a poor approximation of the actual physical system. The control-based continuation approach overcomes both of these challenges, provided that it is suitably initialized (e.g., by using a stable

response, as in [31]).

Notably, in a nonlinear system, the periodic response is typically not harmonic. In this case, the reference signals used in the feedback formulation must account for additional harmonics in the Fourier expansion. In Chap. 4, we relied on the fact that only the fundamental harmonic was present in choosing to use four evenly distributed samples per period in the MATLAB `fft` function. With additional harmonics in the response, it becomes necessary to include more samples per period. In a nonlinear system, it might therefore be useful to develop an adaptive algorithm that updates the sampling interval to avoid the potential for aliasing while still minimizing the number of measurements (cf. Chap. 19 of [10]).

Similarly, while the feedback gains were chosen and then held fixed during continuation, a nonlinear application would typically require that the gains be updated along the solution manifold, for example, to accommodate changes to the local stability of a periodic trajectory [20]. Additionally, the continuation paradigm could be coupled to an optimization algorithm that seeks to locate the optimal value of the objective function (e.g., [12]).

Another possible application of control-based continuation is hybrid substructuring [5]. Here, a physical system is broken down into multiple parts. Some parts are modeled on a computer, whereas others are realized in an experiment. Coupling between the simulated parts and the experiment is achieved using actuators and sensors. This allows a hybrid substructuring experiment to be performed without recreating the entire physical system. In fact, [30] proposes a formulation of the control-based continuation paradigm for analyzing the periodic trajectories in a nonlinear substructured system that eliminates the negative effects of delay that are otherwise present in hybrid substructured experiments.

APPENDIX A

CONTINEX-COMPATIBLE IMPLEMENTATION OF ELEMENTARY EXPERIMENTS

The MATLAB functions below implement zero functions used in the application in Chap. 5 of CONTINEX to each of the coupled design problems (cf. Appendix B).

```
function [data y] = openloopssystem(data, x, p)
k1      = data.ok1;
k2      = data.ok2;
k3      = data.ok3;
omega0  = data.ox0(1);
current0 = data.ox0(2);
theta0  = data.ox0(3);
b       = data.b;
J       = data.J;
L       = data.L;
Ke      = data.Ke;
eta     = p(1);
R       = p(2);
Kt      = p(3);
v2r     = x(1);
v2i     = x(2);
v3r     = x(3);
v3i     = x(4);
v4r     = x(5);
v4i     = x(6);
th      = x(7);
T       = 2*pi/eta;
tstart  = 0;
tsam    = 20*T;
tstep   = T/4;
simout  = sim('simopenloopssystem', 'SrcWorkspace', ...
             'current');
omega   = simout.get('omega');
```

```

current = simout.get('current');
theta   = simout.get('theta');
data.x0 = [omega(end); current(end); theta(end)];
tsize   = numel(theta);
fomega  = fft(omega(tsize-4:tsize-1)); %4pts
y       = [v2r-real(fomega(2))/2; ...
          v2i-imag(fomega(2))/2];
fcurrent = fft(current(tsize-4:tsize-1)); %4pts
y       = [y; v3r-real(fcurrent(2))/2; ...
          v3i-imag(fcurrent(2))/2];
ftheta  = fft(theta(tsize-4:tsize-1)); %4pts
y       = [y; v4r-real(ftheta(2))/2; ...
          v4i-imag(ftheta(2))/2];
y       = [y; v4i*cos(th)-v4r*sin(th)];
end

```

```

function [data y] = openloopssystemcont(data, x, p)
k1       = data.ok1;
k2       = data.ok2;
k3       = data.ok3;
omega0   = data.ox0(1);
current0 = data.ox0(2);
theta0   = data.ox0(3);
b        = data.b;
J        = data.J;
L        = data.L;
Ke       = data.Ke;
eta      = p(1);
R        = p(2);
Kt       = p(3);
v2r      = x(1);
v2i      = x(2);
v3r      = x(3);
v3i      = x(4);
v4r      = x(5);
v4i      = x(6);
T        = 2*pi/eta;
tstart   = 0;
tsam     = 20*T;
tstep    = T/4;
simout   = sim('simopenloopssystem', ...
              'SrcWorkspace', 'current');

```

```

omega    = simout.get('omega');
current  = simout.get('current');
theta    = simout.get('theta');
data.x0  = [omega(end); current(end); theta(end)];
tsize    = numel(theta);
fomega   = fft(omega(tsize-4:tsize-1)); %4pts
y        = [v2r-real(fomega(2))/2; ...
            v2i-imag(fomega(2))/2];
fcurrent = fft(current(tsize-4:tsize-1)); %4pts
y        = [y; v3r-real(fcurrent(2))/2; ...
            v3i-imag(fcurrent(2))/2];
ftheta   = fft(theta(tsize-4:tsize-1)); %4pts
y        = [y; v4r-real(ftheta(2))/2; ...
            v4i-imag(ftheta(2))/2];

```

end

```

function [data y] = closeloopssystem(data, x, p)
k1       = data.ck1;
k2       = data.ck2;
k3       = data.ck3;
omega0   = data.cx0(1);
current0 = data.cx0(2);
theta0   = data.cx0(3);
b        = data.b;
J        = data.J;
L        = data.L;
Ke       = data.Ke;
eta      = p(1);
R        = p(2);
Kt       = p(3);
v2r      = x(1);
v2i      = x(2);
v3r      = x(3);
v3i      = x(4);
v4r      = x(5);
v4i      = x(6);
mag      = x(7);
T        = 2*pi/eta;
tstart   = 0;
tsam     = 20*T;
tstep    = T/4;
simout   = sim('simcloseloopssystem', 'SrcWorkspace', ...

```

```

        'current');
omega    = simout.get('omega');
current  = simout.get('current');
theta    = simout.get('theta');
data.x0  = [omega(end); current(end); theta(end)];
tsize    = numel(omega);
fomega   = fft(omega(tsize-4:tsize-1)); %4pts
y        = [v2r-real(fomega(2))/2; v2i-imag(fomega(2))/2];
fcurrent = fft(current(tsize-4:tsize-1)); %4pts
y        = [y; v3r-real(fcurrent(2))/2; ...
           v3i-imag(fcurrent(2))/2];
ftheta   = fft(theta(tsize-4:tsize-1)); %4pts
y        = [y; v4r-real(ftheta(2))/2; ...
           v4i-imag(ftheta(2))/2];
y        = [y; (abs(fomega(2)/2))^2-mag];
end

```

APPENDIX B

IMPLEMENTATION OF COUPLED CONTINUATION PROBLEMS USING CONTINEX

The MATLAB commands shown below were used to analyze the three coupled design problems using the COCO-compatible CONTINEX toolbox (cf. Appendix A).

B.1 Constant Gain Margin

The commands below use the CONTINEX toolbox and the `coco` entry point function to generate the one-dimensional solution manifold associated with the constant gain margin problem (see Fig. 5.1).

```
>> data = struct('ok1', 10, 'ok2', 10, 'ok3', 10, ...
    'ck1', 10, 'ck2', 10, 'ck3', 10, 'b', 1, ...
    'J', 0.4, 'L', 10, 'Ke', 1, 'ox0', [0; 0; 0 ], ...
    'cx0', [0; 0; 0 ]);
>> u_open = chart_phsco.x(1:10);
>> u_close = chart_maxmu.x(1:10);
>> p10=u_open(1:3);
>> x10=u_open(4:10);
>> p20=u_close(1:3);
>> x20=u_close(4:10);
>> prob = coco_prob();
>> prob = coco_set(prob, 'all', 'TOL', 1e-5);
>> prob = coco_set(prob, 'cont', 'ItMX', -2000, ...
    'h_max', 10, 'NPR', 1);
>> prob = coco_set(prob, 'corr', 'ItMX', 1000);
>> prob = coco_set(prob, 'continex', 'NJac', 20);
>> prob = coco_set(prob, 'continex', 'Jach', [0.05 0.05]);
>> prob = continex_isol2sol(prob, 'phi1', ...
    @openloopssystemcont, 'fpar', data, x10, p10);
>> prob = continex_isol2sol(prob, 'phi2', ...
```



```

        @closeloopssystemcont, 'fpar', data, x20, p20);
>> prob = continex_isol2sol(prob, 'phi3', ...
        @closeloopssystemcont, 'fpar', ...
        data, x20, p20+[-0.01;0;0]);
>> prob = coco_add_func(prob, 'phi4', @closeloopdiff, ...
        data, 'zero', 'uidx', [18 28]);
>> prob = coco_add_func(prob, 'phi5', ...
        @closeloopdist, data, 'zero', 'uidx', [17 27]);
>> prob = coco_add_func(prob, 'psi1', @amplitude, data, ...
        'inactive', 'sqmag', 'uidx', [5 6]);
>> prob = coco_add_glue(prob, 'glue1', [9 10], [19 20]);
>> prob = coco_add_glue(prob, 'glue2', [9 10], [29 30]);
>> prob = coco_add_pars(prob, 'pars', [7 9 10 15], ...
        {'phase', 'R', 'Kt', 'mu'});
>> prob = coco_set_parival(prob, 'sqmag', 0.3808^2);
>> prob = coco_set_parival(prob, 'phase', -pi);
>> coco(prob, 'P1MuRkt_CONTINEX_N', [], 1, ...
        {'mu' 'Kt' 'R'}, {[0 5], [1 300], [0.1 300]});

```

B.2 Constant Phase Margin

The commands below use the CONTINEX toolbox and the `coco` entry point function to generate the one-dimensional solution manifold associated with the constant phase margin problem (see Fig. 5.2).

```

>> data = struct('ok1', 10, 'ok2', 10, 'ok3', 10, ...
        'ck1', 10, 'ck2', 10, 'ck3', 10, 'b', 1, ...
        'J', 0.4, 'L', 10, 'Ke', 1, ...
        'ox0', [0; 0; 0 ], 'cx0', [0; 0; 0 ]);
>> u_open = chart_phsco.x(1:10);
>> u_close = chart_maxmu.x(1:10);
>> p10 = u_open(1:3);
>> x10 = u_open(4:10);
>> p20 = u_close(1:3);
>> x20 = u_close(4:10);
>> prob = coco_prob();
>> prob = coco_set(prob, 'all', 'TOL', 1e-5);
>> prob = coco_set(prob, 'cont', 'PtMX', ...
        2000, 'NPR', 1, 'TrMX', 5, 'h_max', 1, ...
        'h_min', 0.001, 'h0', 0.05);

```

```

>> prob = coco_set(prob, 'corr', 'ItMX', 80);
>> prob = coco_set(prob, 'continex', 'NJac', 10);
>> prob = coco_set(prob, 'continex', ...
    'JacH', [0.01 0.01]);
>> prob = continex_isol2sol(prob, 'phi1', ...
    @openloopssystemcont, 'fpar', data, x10, p10);
>> prob = continex_isol2sol(prob, 'phi2', ...
    @closeloopssystemcont, ...
    'fpar', data, x20, p20);
>> prob = continex_isol2sol(prob, 'phi3', 'fpar', ...
    @closeloopssystemcont, ...
    data, x20, p20+[-0.01;0;0]);
>> prob = coco_add_func(prob, 'phi4', ...
    @closeloopdiff, data, 'zero', ...
    'uidx', [18 28]);
>> prob = coco_add_func(prob, 'phi5', ...
    @closeloopseqdist, data, ...
    'zero', 'uidx', [17 27]);
>> prob = coco_add_func(prob, 'psil', ...
    @amplitude, data, 'inactive', ...
    'sqmag', 'uidx', [5 6]);
>> prob = coco_add_glue(prob, 'glue1', ...
    [9 10], [19 20]);
>> prob = coco_add_glue(prob, 'glue2', ...
    [9 10], [29 30]);
>> prob = coco_add_pars(prob, 'pars', ...
    [7 9 10 15], {'phase', 'R', 'Kt', 'mu'});
>> prob = coco_set_parival(prob, 'sqmag', 1);
>> prob = coco_set_parival(prob, 'phase', -0.1099);
>> coco(prob, 'P2MuRkt_CONT.P', [], 1, ...
    {'mu' 'Kt' 'R'}, {[0 5], [1 300], [0.1 300]});

```

B.3 Constant Nyquist Distance

The commands below use the CONTINEX toolbox and the `coco` entry point function to generate the one-dimensional solution manifold associated with the constant Nyquist distance problem (see Fig. 5.3).

```

>> data = struct('ok1', 10, 'ok2', 10, 'ok3', 10, ...
    'ck1', 10, 'ck2', 5, 'ck3', 10, 'b', 1, ...

```

```

        'J', 0.4, 'L', 10, 'Ke', 1, 'ox0', [0; 0; 0 ],...
        'cx0', [0; 0; 0 ]);
>> u_open = chart_othco.x(1:9);
>> u_close = chartmaxmu.x(1:10);
>> x110 = u_open(4:9);
>> p110 = u_open(1:3);
>> x120 = u_open(4:9);
>> p120 = u_open(1:3)+[-0.01;0;0];
>> x20 = u_close(4:10);
>> p20 = u_close(1:3);
>> prob = coco_prob();
>> prob = coco_set(prob, 'all', 'TOL', 1e-6);
>> prob = coco_set(prob, 'cont', 'PtMX', -2000, ...
        'NPR', 1, 'TrMX', 5, 'h_max', 10, ...
        'h_min', 0.01, 'h0', 0.05)
>> prob = coco_set(prob, 'corr', 'ItMX', 200);
>> prob = coco_set(prob, 'continex', 'NJac', 10);
>> prob = coco_set(prob, 'continex', 'JacH', [0.01 0.01]);
>> prob = continex_isol2sol(prob, 'phi1', ...
        @openloopssystempcont, 'fpar', data, ...
        x110, p110);
>> prob = continex_isol2sol(prob, 'phi2', ...
        @openloopssystempcont,...
        'fpar', data, x120, p120);
>> prob = continex_isol2sol(prob, 'phi3', ...
        @closeloopssystemcont,...
        'fpar', data, x20, p20);
>> prob = continex_isol2sol(prob, 'phi4', ...
        @closeloopssystemcont,...
        'fpar', data, x20, p20+[-0.01; 0; 0]);
>> prob = coco_add_func(prob, 'phi5', ...
        @closeloopdiff, data, ...
        'zero', 'uidx', [26 36]);
>> prob = coco_add_func(prob, 'phi6', @etadif, ...
        data, 'zero', 'uidx', [7 16]);
>> prob = coco_add_func(prob, 'phi7', ...
        @closeloopseqdist, data, ...
        'zero', 'uidx', [23 33]);
>> prob = coco_add_func(prob, 'psi1', ...
        @distnyq, data, 'inactive', ...
        'sqdist', 'uidx', [5; 6]);
>> prob = coco_add_func(prob, 'psi2', ...
        @othnyq, data, 'inactive', '...

```

```

    oth', 'uidx', [5; 6; 14; 15]);
>> prob = coco_add_glue(prob, 'glue1', [8 9], [17 18]);
>> prob = coco_add_glue(prob, 'glue2', [8 9], [27 28]);
>> prob = coco_add_glue(prob, 'glue3', [8 9], [37 38]);
>> prob = coco_add_glue(prob, 'glue4', [8 9], [46 47]);
>> prob = coco_add_pars(prob, 'pars', [8 9 23], ...
    {'R', 'Kt', 'mu'});
>> prob = coco_set_parival(prob, 'sqdist', 0.36);
>> prob = coco_set_parival(prob, 'oth', 0);
>> coco(prob, 'P3MuRkt_CONT.N', [], 1, {'mu' 'Kt' 'R'}, ...
    {[0 5], [1 300], [0.1 300]});

```

REFERENCES

- [1] Bandyopadhyay, M.N., 2002. *Control Engineering: Theory and Practice*. PHI Learning Pvt. Ltd..
- [2] Barton, D.A. and Burrow, S.G., 2011. “Numerical continuation in a physical experiment: investigation of a nonlinear energy harvester,” *Journal of Computational and Nonlinear Dynamics*, 6(1), p. 011010.
- [3] Barton, D.A., Mann, B.P. and Burrow, S.G., 2012. “Control-based continuation for investigating nonlinear experiments,” *Journal of Vibration and Control*, 18(4), pp. 509-520.
- [4] Barton, D.A. and Sieber, J., 2013. “Systematic experimental exploration of bifurcations with noninvasive control,” *Physical Review E*, 87(5), p. 052916.
- [5] Botelho, R.M. and Christenson, R.E., 2014. “Mathematical Framework for Real-Time Hybrid Substructuring of Marine Structural Systems,” *In Dynamics of Civil Structures*, Volume 4, pp. 175-185.
- [6] Bureau, E., Schilder, F., Santos, I., Thomsen, J.J. and Starke, J., 2011. “Experimental bifurcation analysis for a driven nonlinear flexible pendulum using control-based continuation,” in *Proceedings of 7th European Nonlinear Dynamics Conference*, Rome, Italy.
- [7] Bureau, E., Santos, I.F., Thomsen, J.J., Schilder, F. and Starke, J., 2012. “Experimental Bifurcation Analysis by Control-Based Continuation: Determining Stability,” in *Proceedings of ASME 2012 International Design Engineering Technical Conferences and Computers and Information in Engineering Conference*, pp. 999-1006. Chicago, Illinois.
- [8] Bureau, E., Schilder, F., Elmegård, M., Santos, I.F., Thomsen, J.J. and Starke, J., 2014. “Experimental bifurcation analysis of an impact oscillator-Determining stability,” *Journal of Sound and Vibration*, 333(21), pp. 5464-5474.
- [9] Bureau, E., Schilder, F., Santos, I., Thomsen, J.J. and Starke, J., 2014. “Experiments in nonlinear dynamics using control-based continuation:

- Tracking stable and unstable response curves,” in Proceedings of 8th European Nonlinear Dynamics Conference, Vienna, Austria.
- [10] Dankowicz, H. and Schilder, F., 2013. *Recipes for Continuation*. SIAM.
- [11] Franklin, G.F., Powell, J.D., Emami-Naeini, A. and Powell, J.D., 1994. *Feedback Control of Dynamic Systems* Volume 3. Reading, MA: Addison-Wesley.
- [12] Kernévez, J.P., Liu, Y., Seoane, M.L. and Doedel, E.J., 1990. “Optimization by continuation,” In *Continuation and Bifurcations: Numerical Techniques and Applications* (pp. 349-362). Springer Netherlands.
- [13] Leonides, C.T. ed., 2012. *Multidisciplinary Engineering Systems: Design and Optimization Techniques and Their Application: Advances in Theory and Applications*. Academic Press.
- [14] Lipták, B.G. ed., 2005. *Instrument Engineers’ Handbook*, Volume 2. CRC press.
- [15] MacFarlane, A.G.J. ed., 1979. *Frequency-Response Methods in Control Systems*. New York: IEEE Press.
- [16] Marschler, C., Sieber, J., Berkemer, R., Kawamoto, A. and Starke, J., 2014. “Implicit methods for equation-free analysis: convergence results and analysis of emergent waves in microscopic traffic models,” *SIAM Journal on Applied Dynamical Systems*, 13(3), pp.1202-1238.
- [17] Marschler, C., Sieber, J., Hjorth, P.G. and Starke, J., 2015. “Equation-free analysis of macroscopic behavior in traffic and pedestrian flow,” in *Proceedings of Traffic and Granular Flow ’13*, pp. 423-439. Springer.
- [18] MathWorks, ”DC Motor Control,” (2017, Apr. 18), [Online], Available: <https://www.mathworks.com/help/control/examples/dc-motor-control.html>.
- [19] Michalewicz, Z. and Schoenauer, M., 1996. “Evolutionary algorithms for constrained parameter optimization problems,” *Evolutionary computation*, 4(1), pp. 1-32.
- [20] Misra, S., Dankowicz, H. and Paul, M.R., 2008. “Event-driven feedback tracking and control of tapping-mode atomic force microscopy,” *Proceedings of the Royal Society of London A: Mathematical, Physical and Engineering Sciences*, Volume 464, No. 2096, pp. 2113-2133).
- [21] Krauskopf, B. and Sieber, J., 2014. “Bifurcation analysis of delay-induced resonances of the El-Nino Southern Oscillation,” *Proceedings of the Royal Society of London A: Mathematical, Physical and Engineering Sciences*, Volume 470, p. 20140348.

- [22] Pil, A.C. and Asada, H.H., 1996. "Integrated structure/control design of mechatronic systems using a recursive experimental optimization method," *IEEE/ASME Transactions on Mechatronics*, 1(3), pp. 191-203.
- [23] Renson, L., Gonzalez-Buelga, A., Barton, D.A.W. and Neild, S.A., 2016. "Robust identification of backbone curves using control-based continuation," *Journal of Sound and Vibration*, 367, pp. 145-158.
- [24] Rigatos, G., 2011. *Modelling and Control for Intelligent Industrial Systems: Adaptive Algorithms in Robotics and Industrial Engineering*. Volume 7. Springer.
- [25] Rugh, W.J., 1993. *Linear System Theory*. Second Edition. Upper Saddle River, NJ: Prentice Hall.
- [26] Sieber, J. and Krauskopf, B., 2007. "Control-based continuation of periodic orbits with a time-delayed difference scheme," *International Journal of Bifurcation and Chaos*, 17(08), pp. 2579-2593.
- [27] Schilder, F., Bureau, E., Santos, I.F., Thomsen, J.J. and Starke, J., 2015. "Experimental bifurcation analysis-Continuation for noise-contaminated zero problems," *Journal of Sound and Vibration*, 358, pp. 251-266.
- [28] Schilder, F., Bureau, E., Starke, J., Dankowicz, H., and Sieber, J. 2011. "A Matlab Continuation Toolbox for Response Tracking in Experiments," in *Proceedings of 7th European Nonlinear Dynamics Conference*, Rome, Italy.
- [29] Sieber, J. and Krauskopf, B., 2008. "Control based bifurcation analysis for experiments," *Nonlinear Dynamics*, 51(3), pp. 365-377.
- [30] Sieber, J. and Krauskopf, B., 2008. "Tracking oscillations in the presence of delay-induced essential instability," *Journal of Sound and Vibration*, 315(3), pp. 781-795.
- [31] Sieber, J., Gonzalez-Buelga, A., Neild, S.A., Wagg, D.J. and Krauskopf, B., 2008. "Experimental continuation of periodic orbits through a fold," *Physical Review Letters*, 100(24), p. 244101.
- [32] Sieber, J., Krauskopf, B., Wagg, D., Neild, S. and Gonzalez-Buelga, A., 2011. "Control-based continuation of unstable periodic orbits," *Journal of Computational and Nonlinear Dynamics*, 6(1), p. 011005.
- [33] William, S.L., 1999. *Control System Fundamentals*. CRC Press.